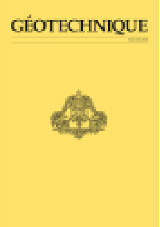

Géotechnique

Modelling the infiltration behavior of foam into saturated sand considering capillary resistance for EPB shield tunneling

GEOT-2021-146 | Paper

Submitted by: Dongzhu Zheng, Adam Bezuijen, Markus Thewes

Keywords: EPB, PHYSICAL MODELLING, FOAM INFILTRATION, FOAM-SOIL INTERACTION, CAPILLARY RESISTANCE

Modelling the infiltration behavior of foam into saturated sand considering capillary resistance for EPB shield tunneling

Dongzhu Zheng [a, *], Adam Bezuijen [a, b], Markus Thewes [c]

[a] *Department of Civil Engineering, Ghent University, Ghent, Belgium*

[b] *Deltares, Delft, The Netherlands*

[c] *Institute for Tunnelling and Construction Management, Ruhr-University Bochum, Bochum, Germany*

[*] *Corresponding author address: Technologiepark 68, Ghent, 9052, Belgium, Tel. +32 9 2645724, Fax. +32 9 2645849, e-mail: dongzhu.zheng@ugent.be*

Abstract

With reference to the Earth Pressure Balance (EPB) shield tunneling, the pressure infiltration of foam into saturated sand is numerically investigated based on experimental analysis. The model accounts for foam spurt during foam infiltration that was experimentally discovered in a previous paper. The maximum penetration depth by foam bubbles is estimated with a simplified micro stability model based on the minimum pressure difference over an individual foam bubble across the pore throats. Although the micro stability model underestimates the maximum penetration depth in one of the sands used, it predicts well with the results obtained for the other two sands. Possible reason for the underestimation in one of the sands is discussed. Further results from numerical simulation are in accordance with the measured discharge behavior during foam spurt. The general agreement suggests that the model could explain the foam flow behavior and can be used to describe foam spurt during foam infiltration that can be expected in EPB shield tunneling.

Key words: EPB, Physical modelling, Foam infiltration, Foam-soil interaction, Capillary resistance

Introduction

The wide application of the EPB shield tunnel-boring machines (TBM) has led to a number of studies in related subjects (Bezuijen & Dias, 2017; Budach & Thewes, 2015; Bezuijen, 2012; Thewes & Budach, 2012; Peila et al., 2009; Merritt & Mair, 2006; Anagnostou & Kovári, 1996). Owing to the development of the soil conditioning technology, the application range of the EPB shield TBM has been extended from clayey soils to coarse-grained soils (Thewes, 2007). Conditioning agents like foam, bentonite and polymer are often used to condition the excavated soil into a low permeable, homogenous plastic paste in order to correctly apply the support pressure onto the tunnel face.

Foam is the most important additive with multiple benefits including the temporary increase of porosity and compressibility as well as decreasing the shear stress and the permeability of the soils (Thewes & Budach, 2012; Psomas, 2001; Bezuijen & Schaminée, 1999). Most research focused on the bulk properties of the conditioned soils such as fluidity (Peila et al., 2009), shear behavior (Psomas, 2001), compressibility (Bezuijen, 2013) and permeability (Borio et al., 2010) and the effect of conditioned soils on the mechanical parts of the machinery such as tool wear (Wei et al., 2019) and rotating torque (Merritt & Mair, 2006). While only limited research can be found regarding the interaction between foam and soils (Xu et al., 2021; Wu et al., 2020; Wang et al., 2020; Galli, 2016).

Bezuijen (2002) proposed a groundwater flow model to predict the excess pore pressure in front of the tunnel face. He compared the field measurement data and found the difference in the maximum pore pressure measured in the soil in front of a slurry shield and an EPB shield is only small. This suggests that the groundwater flow model can be used in both slurry shield and EPB shield. The course of the pore water pressure in the soil for a slurry shield was investigated by Broere and van Tol (2000, 2001) and Bezuijen et al. (2001, 2016). Bezuijen et al. (2001, 2016) assume the formation of an internal and external filter cake. Slurry infiltration has been extensively studied (Xu, 2018; Zizka et al., 2018; Talmon et al., 2013; Min et al., 2013). Although foam infiltration has been studied experimentally by Xu et al. (2021), Galli (2016), Quebaud et al. (1998) and Maidl (1995), the mechanism of foam infiltration remains unclear.

Bezuijen and Dias (2017) developed a model to describe the pressure dissipation in the mixing chamber during standstill of an EPB shield. By fitting the field measurement data to the theoretical model, the permeability of the soils in front of the tunnel face was estimated. It was found that the permeability of the soils predicted by the model is 2 to 3 times smaller than that from field measurements. Indicating that there could be a foam infiltration layer with a high flow resistance that results in the underestimation of the soil permeability by the model of Bezuijen and Dias (2017). The model was employed by Yu et al. (2020) and reasonable agreement was obtained with field measurements during both drilling and standstill.

Galli et al. (2021) conducted a series of experiments on foam penetration into cohesionless soils with the aim to assess the residual water content during drilling of an EPB shield TBM. The penetration process was described qualitatively by regression analysis using the power law model within the testing duration of 3 minutes. Xu et al. (2021) compared the infiltration characteristics between foam and slurry infiltration tests and found that a foam spurt process is also present compared with mud spurt in slurry infiltration. Zheng et al. (2021) found through experiments that the foam spurt results in an internal low permeable layer that creates a large pressure drop over the infiltrated sand. Although there are still fine bubbles migrating further into the sand after foam spurt, most of the bubbles are entrapped among the sand pores near the sand surface and the dominating flow will be the drainage behavior of foam.

The use of foam in EPB shield tunneling is still mainly based on experience over nearly 50 years of development and has not become a standard process regarding its injection strategy. One possible reason may be the lack in the understanding of the foam-soil interaction, of which foam flow in saturated sand plays an important role. With the aim to understand how the foam infiltration could influence the flow behavior during standstill as well as to what extent the low permeable layer with high flow resistance could be formed, a series of foam infiltration experiments was conducted (Zheng et al., 2021). This paper focuses on the model interpretation of the foam infiltration behavior. The model is based on an infiltration model for slurry infiltration (Bezuijen et al., 2016). In addition, a finite permeability of the water through the foam in the sand is assumed. An individual bubble is considered when it penetrates the sand and the limit equilibrium state is described in a simplified micro stability model. A calculation model is developed based on a micro stability model to predict the maximum penetration depth during ‘foam spurt’ (explained in the next section). The calculation model predicts the flow behavior during foam infiltration, which accounts for the bubble flow as well as the flow of the foaming liquid responsible for the drainage of foam. Results are compared with the experimental data and further application is discussed.

Mechanisms during foam infiltration

Analogous to the two processes of mud spurt and filter cake formation for slurry infiltration (Talmon et al., 2013), a comparable foam spurt process was observed by Xu et al. (2020) and it is adopted in this study. It was found by Zheng et al. (2021) that there is a maximum penetration depth by foam bubbles during foam spurt. After foam spurt, the migration of foam bubbles almost stops, and the flow is mainly controlled by the foam infiltrated sand which have the lowest permeability of the whole system. Further infiltration process was found to be the main process after foam spurt. The further infiltration process is somewhat similar to the deep bed filtration during slurry infiltration where bentonite particles are retained in the pores that the permeability of the sand decreases slowly (Yin et al., 2021; Xu & Bezuijen, 2019). The mechanisms may be different because during further infiltration, fine bubbles will not remain in the pores due to adhesion but are entrapped in the pores due to its larger volume compared with the pore throats. During further infiltration, only a small proportion of the foam bubbles at the foam front could be able to travel further and the main flow will be the water flow through the foam infiltrated sand. Besides the bubble infiltration, there is always a liquid flow due to the drainage behavior of the foam. Consequently, there is an invisible liquid front ahead of the foam front (see Figure 1).

Model derivation

In this paper, the flow behaviors during foam spurt as well as the companion liquid flow through the foam in the sand are modelled. After foam spurt, the fine bubbles migrating during further infiltration are not included in the model because it is unable to determine the amount of these fine bubbles. The model is calibrated using the results of experiments, therefore the experimental setup is described.

As shown in Figure 2, x is the penetration depth by the foam bubbles and x' the distance between the foam bubble front and the invisible liquid front. ϕ_1 represents the piezometric head in the foam above the sand surface and ϕ_0 the piezometric head at the foam front. The piezometric head at the bottom of the sand column is taken to be 0.

In this set-up, a small cylinder (with diameter D_2 and length L_{s2}) is added beneath the large cylinder (with diameter D_1 and length L_{s1}) to create an extra flow resistance which makes the equivalent length (L_s) of the sand column equal to 5 m. The hydraulic gradient in the sand column will be $\Delta\phi/Ls = 1$ when the applied pressure is 50 kPa during the test. This is comparable to the hydraulic gradient predicted by the groundwater flow model described in Bezuijen (2002) with a shield diameter of 10 m and an extra pore water pressure of 50 kPa. Detailed explanation can be found in papers by Xu (2018) and Zheng et al. (2021).

Figure 3 shows the experimental results of the infiltration depth against square root of time. The infiltration depth is calculated assuming there is no liquid drainage from the foam and therefore this depth is larger than the actual penetration depth by foam bubbles. It shows that after the initial fast penetration of the foam bubbles, there is a slower discharge period which is approximately linear against square root of time. It was found that the permeability of the foam-infiltrated sand (x in Figure 2) is the lowest in the whole system. There is no impermeable layer formed on top of the sand, but the linear part is related to the layer of low permeability formed during foam spurt. After foam spurt, there is limited foam bubble infiltration and the dominant flow will be the water flow from the foam. The linear line against square root of time is the result of the increase of the foam infiltration layer and therefore can be simulated. There are some different discharge patterns after the linear distribution period for some unknown reasons as can be seen from Figure 3. This paper will only focus on the simulation of foam spurt which comprises the initial fast discharge and the linear discharge against square root of time shown in Figure 3.

As shown for slurry infiltration (Bezuijen et al., 2016), the penetration of slurry into the sand does not follow Darcy's law, because slurry is a fluid with yield stress and a certain pressure drop is necessary to push the slurry further into the sand. The experimental results from Xu (2018) and Zheng et al. (2021) suggest that there is a maximum penetration depth (L) when foam is pressurized into saturated sand, indicating a yield stress in the foam flow. Assume foam to be a Bingham fluid, the flow in porous media can be expressed as follows (Bezuijen et al., 2016):

$$v_f = \frac{k_f}{n}\left(\frac{d\phi}{dx} - i_t\right) \qquad (1)$$

With v_f the penetration velocity of the foam bubbles, k_f the permeability of the sand for foam, n the porosity of the sand and i_t the threshold hydraulic gradient.

The threshold hydraulic gradient (i_t) can be calculated when the maximum penetration depth (L) is known. Specifically, because there is a water flow after the foam has reached its maximum penetration depth, a certain pressure difference over the foam front and the outlet at the maximum penetration depth should be present. The threshold hydraulic gradient (i_t) can be estimated:

$$i_t = \frac{\phi_1 - \phi_{0,end}}{L} \qquad (2)$$

With $\phi_{0,end}$ the piezometric head of the foam front at maximum penetration depth.

Considering there is always a drainage behavior during foam spurt, an extra water flow through the sandy foam should be accounted for in the total discharge.

$$v_{fw} = k_{fw} \frac{\phi_1 - \phi_0}{nx} \qquad (3)$$

With v_{fw} the penetration velocity of water with respect to the penetration velocity of the foam bubbles and k_{fw} the permeability of the sandy foam.

The pore water velocity in the sand ahead of the foam front can be calculated:

$$v = k_s \frac{\phi_0}{n(L_s - x)} \qquad (4)$$

With v the pore water velocity in the sand ahead of the foam front and k_s the permeability of the sand.

The total velocity of the water is the addition of the foam velocity and the water velocity with respect to the foam velocity:

$$v = v_f + v_{fw} \qquad (5)$$

At the maximum penetration depth, the bubble penetration stops ($v_f = 0$), and there will only be a water flow. It comes to the following relation:

$$k_{fw} \frac{\phi_1 - \phi_{0,end}}{L} = k_s \frac{\phi_{0,end}}{L_s - L} \qquad (6)$$

The Equations 1~4 can be solved numerically using an explicit scheme starting from x = 0 at t=0.

The maximum penetration depth (L) can be obtained by analyzing the micro stability of an individual foam bubble across the sand pores. Rossen and Gauglitz (1990) developed a model to describe the minimum pressure gradient of foam flow through porous media. But the pressure difference in their model is between gas and liquid which is more applicable in the field of enhanced oil recovery. While here a model to describe the difference in pore water pressure is needed. Therefore, a simplified micro stability model is proposed to get L.

In the experiments, one fine sand (Sand 1) and two medium sands (Sand 2 and 3) (Figure 4) were tested to represent different sand stratums. The foam expansion ratio (FER) of the foam used in the experiments were 10, 15 and 20. Grain (bubble) size distribution curves of the three types of sand (foam) are shown in Figure 4. It should be mentioned that the bubble size is measured at atmospheric pressure and calculated at an absolute pressure of 1.5 bar according to Boyle's Law. The volume of an individual bubble will increase as it travels further due to the decrease in its surrounding pore water pressure. The compressibility in this case will be discussed in the following part.

The filter rule derived by Terzaghi and regulated in USACE (2000) is a common guidance for filter design in dams and dikes. A filter material is placed downstream to prevent particle loss of the base material. A major criterion for the filter material is $D_{15}/d_{85} \leqslant 4$ (D_{15} for the filter material and is the diameter which 15% of the filter material's mass content smaller than, d_{85} for the base material). Assume the foam being a base material with the same gradation and the sand column being a filter material, the potential of particle loss from the base material into the filter material is first checked with the filter rule. A regular base material is different to foam because sand particles cannot deform like foam bubbles. If it fulfills the filter rule, there would hardly be any transportation of foam bubbles into the pore space of the sand column without changing shapes. The related values are summarized in Table 1. It shows that the combinations of different base and filter materials fulfil the filter rule, suggesting that no bubble penetration could take place without changing its shape.

Figure 5 shows a sketch of shape changes in a bubble penetration over an individual pore throat. The changes in shape require a pressure difference to initiate the deformation which is related to the geometry of the pore throat and the surface tension of the bubble. Here the mechanism is first discussed in general and the determination of relevant parameters will be introduced subsequently.

As illustrated in Figure 5, the bubble changes from position A to B and C. A', B' and C' represent the bottom part of the bubble at corresponding moments, respectively. The pore water pressure on top of the bubble is P_{w1} and at the bottom P_{w2}. The difference in pore water pressure on either side of the pore throat (P_{w1}-P_{w2}) pushes the bubble downwards that the bottom part bulges through the pore throat.

Because the surface tension resists the forward movement during the change from *A'* to *B'*, the capillary pressure will be the largest at the narrowest position *B'* where the bottom part of the bubble has the largest curvature. The movement will carry on from B to C when the pressure difference (P_{w1}-P_{w2}) can overcome this largest capillary pressure. Because position *B*-*B'* is very crucial to a bubble penetration, it will be analyzed based on its equilibrium state.

By the definition of surface tension (γ), the following relations can be obtained:

$$P_a - P_{w1} = \frac{4\gamma}{D} \qquad (7)$$

$$P_a - P_{w2} = \frac{4\gamma}{d} \qquad (8)$$

With *D* the local diameter on top of the bubble and *d* the throat diameter.

Combining Equation 7 and 8 yields:

$$P_{w1} - P_{w2} = 4\gamma(\frac{1}{d} - \frac{1}{D}) \qquad (9)$$

Equation (9) represents the minimum difference in pore water pressure for a bubble to travel through an individual pore throat. Above this pressure difference, the bubble will continue to penetrate further. At the maximum penetration depth (*L*), the pressure difference will no longer be able to push the bubble forward and the penetration will stop.

There can be two different conditions regarding the sizes between the bubble and the pore body with the values listed in Table 1, as shown in Figure 6, these two conditions mainly influence the local diameter on top of the bubble (*D*).

1) The bubble size is equal to or smaller than the pore body (Fig. 4a) but bigger than the throat diameter (sand 3-FER 10). In this case, a bubble can fully pass through an individual throat before it starts the next penetration. The pressure drop over one foam bubble is equal to the pressure difference over one pore throat. *D* in this case will be taken as the average diameter of the bubbles. The diameter of the bubble is influenced by the pore water pressures at different vertical locations. Assume *i* (starting from *i* =1) to be the number of bubble penetrations along the flow direction. The pressure drop in one bubble penetration is:

$$P_{wi} - P_{w(i+1)} = 4\gamma(\frac{1}{d} - \frac{1}{D_i}) \quad (10)$$

With i the number of bubble penetrations across the pore throat and D_i the diameter at that point which can be calculated according to Boyle's law:

$$D_{(i+1)} = \sqrt[3]{\frac{P + P_{wi}}{P + P_{w(i+1)}}} D_i \quad (11)$$

With P the atmospheric pressure.

The calculation scheme stops when $P_{w(i+1)} <= 0$. Assuming the pore space to be equal to the diameter of the sand grains, the maximum penetration depth can be calculated by:

$$L = MD_s \quad (12)$$

With M the maximum value of i and D_s the average diameter of the sand grains.

The calculation scheme described by Equations 10 to 12 can be carried out starting from i =1, $D_1 = D$ and P_{w1} = 50 kPa.

2) The bubble size is bigger than the pore body (Fig.4b). An individual bubble needs to take up more than one pore throat at a time that the bubble flows as 'bubble trains' during penetration (Rossen, 1990). In this case, a volume factor (α) is introduced to represent the number of pore throats occupied by one bubble. The volume of bubble can be calculated when the pore water pressure is known. A simplification in this model takes the local diameter on top of the bubble to be equal to the pore space which is equal to the diameter of the sand grains, the pressure drop in one bubble penetration is:

$$P_{wi} - P_{w(i+1)} = 4\gamma(\frac{1}{d} - \frac{1}{D}) \quad (13)$$

The number of bubbles along the infiltration path can be obtained by:

$$N = \frac{\Delta P}{P_{wi} - P_{w(i+1)}} \quad (14)$$

With N the number of bubbles along the maximum penetration depth and ΔP the total excess pore pressure.

Since the volume of bubble is inversely proportional to the absolute pressure, the volume factor for bubbles at different places along the penetration path can be obtained and the maximum penetration depth is:

$$L = D\sum_{i=1}^{N}\alpha \frac{P+\Delta P}{P+[\Delta P-(i-1)\frac{\Delta P}{N}]} \quad (15)$$

With α the volume factor that is determined by the volume ratio between the bubble and the pore space.

Here d_{10} ($d_{10,s}$ for sand and $d_{10,f}$ for foam) is taken to be the characteristic values that are summarized in Table 2.

Results and discussion

Maximum penetration depth

The surface tension (γ) of the foaming liquid was measured with a single capillary tube with an inner diameter of 0.15 mm and outer diameter of 0.25 mm and a length of 300 mm (CM Scientific, CV1525 Borosilicate Glass Round Capillaries) at room temperature of 20 °C. The measurement was also conducted with water as a reference. Measurement results are listed in Table 3.

The measurement result on water is very close to standard value of 0.07275 N/m (Vargaftik et al., 1983), indicating the reliability of the capillary rise method.

The throat diameter of the sand was determined by the measured water retention curve. Water retention curve was measured using the hanging water column test in which suction pressures were varied by adjusting the height of the water column in a stepwise manner (see Lins, 2009). The testing method has the advantage of its ability to obtain very small suction pressure among a small pressure range since sand usually presents a relatively small range of air entry values (Lins, 2009). During the measurement, air will displace the water in the pore space as long as the pressure difference could overcome the capillary pressure. As indicated in Figure 5, the capillary pressure is the largest at the narrowest point with the throat diameter d. Therefore, the measured water retention curve has a relation with the throat diameter. The measurement data can be fitted to the van Genuchten model (1980):

$$\Theta = \left[\frac{1}{1+(ah)^n}\right]^m \quad (16)$$

With Θ the normalized volumetric water content, a, n and m=1-1/n curve fitting soil parameters and h the pressure head.

The range of air entry values for each sand can be obtained statistically:

$$P - P_w = \frac{4\gamma_w}{d} \qquad (17)$$

with P the atmospheric pressure, P_w the suction pressure (negative) and γ_w the surface tension of water.

Take Sand 1 as an example, the air entry value is between 3.2~12 kPa and the calculated throat diameter is between 0.024~0.091 mm. The pore space for each sand is considered to be the same to its characteristic grain size. With the maximum and minimum throat diameter, a distribution curve regarding the throat diameter can be developed with different air entry values and their corresponding volumetric water contents. The results are shown in Figure 7.

With the distribution curve, $d_{10,p}$ is taken to be the characteristic throat diameter and the values for each sand are listed in Table 2. The Terzaghi model assumes the throat diameter ($d_{10,p}$) to be approximately one quarter of the characteristic grain size ($d_{10,s}$). While the ratio of $d_{10,p}$ / $d_{10,s}$ can be found in Table 2 and it is 0.29, 0.42 and 0.27 for Sand 1, Sand 2 and Sand 3, respectively. It can be seen that only for Sand 2, the ratio is apparently different from the Terzaghi value of 0.25, which could be induced by its relative density of 70%. For Sand 1 and Sand 3, it is quite close (0.29 and 0.27 for Sand 1 and Sand 3, respectively) at the relative density of 80%.

Table 2 shows that the micro stability model predicts well compared with the experimental results for Sand 1 and Sand 2. The model underpredicts the maximum infiltration depth for Sand 3, probably because finer bubbles are smaller than the larger pore throats in Sand 3 and thus are simply transported. Although Table 1 shows that there is no bubble penetration without changing its shape with the filter rule, Figure 4 and Figure 7 show that a certain proportion of foam bubbles are smaller than the measured largest pore throats in Sand 3. For foam FER of 10, this proportion is about 70% and about 60 % and 40 % for foam FER of 15 and 20, respectively. As a consequence, the multiple number of bubbles in a single pore space likely result in the bubbles being more or less connected, which results in a smaller pressure drop over an individual pore throat than the model prediction.

Model simulation

The permeability of the sandy foam for water (k_{fw}) can be determined according to Darcy's Law:

$$k_{fw} = \frac{\Delta L Q}{A_C \Delta \phi} \tag{18}$$

With ΔL the distance between two adjacent pressure transducers and $\Delta \phi$ the corresponding difference in piezometric head. The distance (ΔL) between k1 and k2 is only 2 cm because the first 2 cm is pure foam. For $k_{2\text{-}3}$ and $k_{3\text{-}4}$ this distance is also 2 cm while for $k_{4\text{-}5}$ it is 4 cm.

At the maximum penetration depth, the bubbles will reach an equilibrium state which is described in the micro stability model. At the equilibrium state, the measured pore pressures by adjacent transducers can be used to calculate the permeability of the sandy foam, because there is only a water flow.

Figure 8 shows the calculated permeabilities with Equation 18. The infiltration depth on the horizontal axis was calculated assuming there was no liquid drainage from the foam and therefore is larger than the actual penetration depth by the bubbles. It shows the calculated values exhibit decreases in permeabilities by several orders of magnitude after the foam bubbles penetrated the corresponding sand layers. For $k_{1\text{-}2}$ this decrease happens at the beginning of the test because the foam bubbles immediately penetrate the sand pores when the test starts. The values of $k_{2\text{-}3}$ kept constant for some infiltration depth, after which they also presented a sharp decrease. A similar situation applies to $k_{3\text{-}4}$, but only after the foam front has penetrated the sand layer sandwiched by k3 and k4. Some fluctuations of $k_{4\text{-}5}$ were observed at the later part of the tests, which is attributed to the small water discharge at the later stage when the accuracy of the pressure transducers and the discharge rate started to influence the results. It should be mentioned that the theoretical infiltration depth at which $k_{2\text{-}3}$ and $k_{3\text{-}4}$ start to decrease for the test with Sand 1 FER 10 should be 0.02 m and 0.04 m, respectively. While these two values are 0.04 m and 0.065 m as shown in Figure 8, larger than the theoretical values. It suggests that the drainage from foam has resulted in a larger infiltration depth when calculated with the discharged water. Similar condition applies to other tests shown in Figure 8.

Before the foam bubbles penetrate the sand pores, the calculated values by Equation 18 should be constant and they should reflect the permeability of the sand sample. Table 4 shows a good compliance when comparing the sand parameters and the calculated constant values from Figure 8.

Basic requirements should be applied when employing the permeability of the sandy foam (k_{fw})

calculated by Equation 18 in the numerical model:

1) The foam bubbles stop penetrating further. This criterion can be roughly met when the maximum penetration depth described in the micro stability model is reached. Although some local unstable state can be expected during the further infiltration process, most part of the foam bubbles in the sand are stranded and the calculated values by Equation 18 will be regarded as the permeability of the sandy foam (k_{fw}).

2) The sand layer sandwiched by adjacent pressure transducers is fully penetrated by the foam bubbles. This is to ensure that the seepage length through sandy foam is equal to the distance between the adjacent transducers when criterion 1 is satisfied and can be distinguished from Figure 8. For instance, when $k_{4\text{-}5}$ starts decreasing, then the sand layer between k3 and k4 is fully infiltrated by the bubbles because now the bubbles have reached beyond k4.

Following the above discussions, k_{fw} was chosen to be around 2×10^{-8} m/s for the test with Sand 1 FER 10 according to Figure 8. The values for other cases are listed in Table 4.

Another parameter that needs to be obtained for the numerical model is the permeability of the sand for foam (k_f). Since it is unrealistic to obtain through measurement, k_f was determined by fitting the measurement data into the simulation results.

The fitting procedure starts from k_f and then both L (from the micro stability model) and k_{fw} (from Figure 8) can be slightly adjusted if model output can better fit into the experimental results. The resulting L can be found in Table 2 and the permeabilities in Table 4. It should be mentioned that the changes in parameters are manual to get better outputs compared with experimental results.

Results from both experiments and model simulation are plotted in Figure 9. It turns out that the simulation yields good agreements with L of 0.09 m with tests of Sand 3. For Sand 1 and Sand 2, the maximum penetration depth (L) fits well with the experimental results except in the test with Sand 2 FER 10, where the value of L is 0.06 m, larger than 0.026 m found in the micro stability model. A possible reason for the underestimation is that 40% of the foam bubbles in foam of FER 10 are smaller than the largest pore throats in Sand 2. The smaller bubbles can simply be transported during the test, which results in a larger penetration depth than the micro stability model prediction. While in general, the good agreements between experiments and model simulation indicate the right physics of the model. It suggests that the model can be used to describe the infiltration behavior during foam spurt which can be expected during EPB shield tunneling.

Figure 10 shows the values of the permeabilities used in the model simulation. With a certain sand type, its permeability to foam is decreasing with an increasing FER. And the permeability of the sandy foam formed during pressure infiltration decreases with an increasing FER. Suggesting that a foam with larger foam bubbles and less water content (bigger FER) results in a lower permeability when infiltrating into the sand. With a coarser sand, its permeability to a certain foam will be larger, which is logical because the throat diameter will be larger in a coarser sand, and it will be easier for both foam bubbles and water to pass through. An interesting point worth further investigation is that all permeabilities decrease by a factor of approximately 2 when FER increases from 10 to 20. A possible reason is that the smaller liquid content in the foam of FER 20 results in the film of the bubbles being thinner, further resulting in a smaller permeability.

Furthermore, the model can be used to calculate the foam infiltration in the tunnel front and the water flow from the mixing chamber during standstill. To do that Equation 3 has to be changed (Bezuijen et al., 2016):

$$v = k_s \frac{\phi_0}{nR} \qquad (19)$$

With R the radius of the tunnel.

Conclusions

This paper presents the model interpretation of the mechanisms during foam infiltration, based on the analysis of the experiments in Zheng et al. (2021). A calculation model is established to describe the flow behavior during foam infiltration into saturated sand tailored to EPB shield tunneling. The model describes the foam bubble flow as well as the companion water flow during foam spurt. The maximum penetration depth by foam bubbles is predicted with a simplified micro stability model. The micro stability model results in good predictions when the foam bubbles are bigger than the pore throat in the sand while it underestimates the maximum penetration depth in other cases (for example, the tests with Sand 2 – FER 10 and Sand 3). Model results show good agreements when compared with experimental results during foam spurt.

The good agreement between the model and experimental results confirms the mechanisms during pure foam infiltration. Although further research is needed for sandy foam infiltration, which seems to be a more realistic situation in an EPB shield, pure foam infiltration is still a possible scenario during standstill as foam is injected through the cutter head to maintain the pressure from time to time. The injection will create a pure foam infiltration which is described in this paper.

Despite the fact that the model neglects the infiltration behavior after foam spurt, it provides a good way to quantify the flow behavior during foam infiltration. Further application of the model can be extended to the prediction of the pore pressures in front of the tunnel face, which could help better understand the pressure development and the foam-soil interaction in EPB shield tunneling. It is therefore recommended to engineers to incorporate the findings of this study in field use of foam for conditioning.

Acknowledgement

The foaming agent used in this study was provided by the Institute for Tunnelling and Construction Management of Ruhr University Bochum. The help from Marius Schroeer and Sascha Freimann is highly appreciated. The soil water retention curve was measured at the Institute for Foundation Engineering, Soil and Rock Mechanics of Ruhr University Bochum, the assistance from Dr. Diethard Koenig is acknowledged. The first author would like to acknowledge the scholarship funded by China Scholarship Council and the CWO Mobility Fund of Ghent University.

Reference

Anagnostou, G. & Kovári K., 1994. The face stability of slurry-shield-driven tunnels. TUST 9 (2): 165-174.

Bezuijen, A., Schaminée, P.E.L. & Kleinjan, J.A., 1999. Additive testing for earth pressure balance shields. Proc. 12th Eur. Conf. on Soil Mech. and Geotech. Engrg., Amsterdam, Balkema, Rotterdam, pp. 1991–1996.

Bezuijen, A., Pruiksma, J.P. & Meerten, H.H., 2001. Pore pressures in front of tunnel, measurements, calculations and consequences for stability of tunnel face. Proc. Int. Symp. on Modern Tunneling Science and Techn. Kyoto.

Bezuijen, A., 2002. The influence of soil permeability on the properties of a foam mixture in a TBM. 4th Int. Symp. on Geotechnical Aspects of Underground Construction in Soft Ground - IS Toulouse 2002.

Bezuijen, A., 2012. Foam used during EPB tunnelling in saturated sand, parameters determining foam consumption. Proc. WTC, Bangkok.

Bezuijen, A., Steeneken, S.P. et al., 2016. Monitoring and analysing pressures around a TBM. In: Proceeding of the 13th International Conference Underground Construction, Prague.

Bezuijen, A. & Dias, T.G.S., 2017. EPB, chamber pressure dissipation during standstill. *EURO: TUN 2017*, Innsbruck University, Austria.

Broere, W. & van Tol A.F., 2000. Influence of Infiltration and Groundwater Flow on Tunnel Face Stability. Geotechnical Aspects of Underground Construction in Soft Ground, Tokyo, Japan, 2000, pp. 339-344.

Broere, W. & van Tol, A.F., 2001. Time-dependant infiltration and groundwater flow in a face stability analysis. In: Proceedings of International Symposium on Modern Tunnelling Science and Technology, Kyoto, pp. 629–634.

Budach, C., Thewes, M., 2015. Application ranges of EPB shields in coarse ground based on laboratory research. Tunnelling and Underground Space Technology, 50: 296-304.

Galli, M., 2016. Bochum Rheological characterisation of Earth-Pressure-Balance (EPB) support medium composed of non-cohesive soils and foam. Doctoral thesis. Ruhr-Universität, Germany.

Galli, M., Thewes, M., Freimann, S. & Schröer, M., 2021. Residual water content of excavated soil in EPB tunnelling. TUST, 114 (2021): 103991. doi.org/10.1016/j.tust.2021.103991

Lins, Y., 2009. Hydro-Mechanical Properties of Partially Saturated Sand. Doctoral thesis. Ruhr-Universität, Germany.

Maidl, U., 1995. Erweiterung der Einsatzbereiche der Erddruckschilde durch Bodenkonditionierung mit Schaum. Doctoral Thesis, Ruhr-Universität Bochum, AG Lei-tungsbau und Leitungsinstandhaltung.

Merritt, A. S. & Mair, R. J. 2006. Mechanics of tunnelling machine screw conveyors: model tests. Géotechnique 56 (9): 605–615.

Min, F., Zhu, W., & Han, X., 2013. Filter cake formation for slurry shield tunneling in highly permeable sand. TUST 38(9): 423-430.

Peila, D., Oggeri, C. & Borio, L., 2009. Using the slump test to assess the behaviour of conditioned soil for EPB tunnelling. Environmental & Engineering Geoscience XV (3): 167–174.

Psomas, S., 2001. Properties of foam/sand mixtures for tunneling applications. Master's thesis, Oxford.

Quebaud, S., Sibai, M. & Henry, J.P., 1998. Use of chemical foam for improvements in drilling by earth pressure balance shields in granular soils. TUST 13 (2): 173-180.

Rossen. W.R. 1990. Theory of Mobilization Pressure Gradient of Flowing Foams in Porous Media. Journal of Colloid and Interface Science 136 (1): 1-16.

Rossen, W.R. & Gauglitz, P.A., 1990. Percolation Theory of Creation and Mobilization of Foams in Porous Media. AIChE J. 36: 1176–1188.

Talmon, A. M., Mastbergen, D. R., & Huisman, M., 2013. Invasion of pressurized clay suspensions into granular soil. Journal of Porous Media 16: 351-365.

Thewes, M., 2007. TBM Tunnelling Challenges—Redefining the State-of-the-Art, Keynote lecture at the 2007 ITA World Tunnel Congress, Prague, Tunel. pp. 13–21.

Thewes, M., Budach, C. & Bezuijen, A., 2012. Foam conditioning in EPB tunneling. Geotechnical Aspects of Underground Construction in Soft Ground. London.

USACE (2000) Engineering Manual 1110-2-1913, Design and Construction of Levees. https://www.publications.usace.army.mil/Portals/76/Publications/EngineerManuals/EM_1110-2-1913.pdf.

van Genuchten, M., 1980. A closed-form equation for predicting the hydraulic conductivity of unsaturated soils. Soil Sci. Soc. Am. J. 44: 892–898.

Vargaftik, N.M., Volkov, B.N. & Voljak, L.D., 1983. International Tables of the Surface Tension of Water. Journal of Physical and Chemical Reference Data. 12 (3): 817-820.

Wang, S., Hu, Q., Wang, H., Thewes, M., Ge, L., Yang, J. & Liu, P., 2021. Permeability Characteristics of Poorly Graded Sand Conditioned with Foam in Different Conditioning States. Journal of Testing and Evaluation. Published ahead of print, September 01, 2021. https://doi.org/10.1520/JTE20190539

Wei, Y., Yang, Y. & Qiu, T., 2019. Effects of Soil Conditioning on Tool Wear for Earth Pressure Balance Shield Tunneling in Sandy Gravel Based on Laboratory Test. Journal of Testing and Evaluation 49. https://doi.org/10.1520/JTE20180851.

Wu, Y., Nazem, A., Meng, F. & Mooney, M.A., 2020. Experimental study on the stability of foam-conditioned sand under pressure in the EPBM chamber. TUST 106 (2020): 103590.

Xu, T., 2018. Penetration and excess pore water pressures in front of a TBM, Experiments, Mechanisms and Computational models. Doctoral thesis. Ghent University, Belgium.

Xu, T. & Bezuijen, A., 2019. Bentonite slurry infiltration into sand: filter cake formation under various conditions. Géotechnique. https://doi.org/10.1680/jgeot.18.P.094

Xu, T., Bezuijen, A. & Thewes, M., 2021. Pressure infiltration characteristics of foam for EPB shield tunnelling in saturated sand – part 1: 'clean' foam. Géotechnique. https://doi.org/10.1680/jgeot.19.P.187

Xu, T., Bezuijen, A. & Thewes, M., 2021. Pressure-infiltration characteristics of foam for EPB shield tunnelling in saturated sand – part 2: soil–foam mixture. Géotechnique. https://doi.org/10.1680/jgeot.19.P.188

Yin, T., Zhang, Z., Huang, X., Shire, T. & Hanley, K.J., 2021. On the morphology and pressure-filtration characteristics of filter cake formation: Insight from coupled CFD–DEM simulations. TUST 111 (2021): 103856. https://doi.org/10.1016/j.tust.2021.103856

Yu, H., Mooney, M. & Bezuijen, A., 2020. A simplified excavation chamber pressure model for EPBM tunneling. Tunnelling and Underground Space Technology 103 (2020): 103457. https://doi.org/10.1016/j.tust.2020.103457

Zheng, D., Bezuijen, A. & Thewes, M., 2021. An experimental study on foam infiltration into saturated sand and its consequence for EPB shield tunneling. TUST, 111 (2021): 103878. https://doi.org/10.1016/j.tust.2021.103878

Zizka, Z., Schoesser, B., Thewes, M., Schanz, T., 2018. Slurry shield tunneling: New methodology for prediction of increased pore pressures resulting from slurry infiltration at the tunnel face under cyclic excavation processes. International Journal of Civil Engineering 7: 113–130.

Tables

Table 1. Values of D_{15}/d_{85} found in different combinations

	Sand 1	Sand 2	Sand 3
Foam 1	0.29	0.28	0.44
Foam 2	0.26	0.28	0.56
Foam 3	0.21	0.22	0.44

Table 2. Parameters found in experiments and model simulation

	FER	$d_{10,s}$ (m)	$d_{10,p}$ (m)	$d_{10,f}$ (m)	Volume factor (α)	L (m)		
						Micro stability model	Model fit	Experiment*
Sand 1	10	1.2×10^{-4}	3.5×10^{-5}	1.8×10^{-4}	4	0.016	0.017	$0< L <0.02$
	15			2.4×10^{-4}	8	0.033	0.036	$0.04< L <0.06$
	20			2.6×10^{-4}	11	0.045	0.045	$0.04< L <0.06$
Sand 2	10	1.3×10^{-4}	5.5×10^{-5}	1.8×10^{-4}	3	0.026	0.06	$0.04< L <0.06$
	15			2.4×10^{-4}	7	0.061	0.061	$0.04< L <0.06$
	20			2.6×10^{-4}	8	0.069	0.069	$0.06< L <0.1$
Sand 3	10	2.6×10^{-4}	7.0×10^{-5}	1.8×10^{-4}	1	0.017	0.09	$0.06< L <0.1$
	15			2.4×10^{-4}	1	0.016	0.09	$0.06< L <0.1$
	20			2.6×10^{-4}	1	0.023	0.09	$0.06< L <0.1$

* Experimental data from Zheng et al. (2021)

Table 3. Measured capillary rise and calculated surface tension

	h (m)	γ (N/m)
water	0.1982	0.0728
Foaming liquid	0.0583	0.0214

Table 4. Permeabilities found in experiments and model simulation

	k_s ($\times10^{-4}$ m/s)		FER 10 ($\times10^{-8}$ m/s)			FER 15 ($\times10^{-8}$ m/s)			FER 20 ($\times10^{-8}$ m/s)		
	k_s (Fig. 8)	k_s *	k_{fw} (Fig.8)	k_{fw}	k_f	k_{fw} (Fig.8)	k_{fw}	k_f	k_{fw} (Fig.8)	k_{fw}	k_f
Sand 1	1.0	1.5	2	2.6	8	2	1.8	4	2	1.5	3
Sand 2	4.0	5.0	2	4.3	42	3	4	30	2	2.3	25
Sand 3	6.0	6.0	15	5.8	80	10	3.6	45	5	2.3	40

* Experimental data from Zheng et al. (2021)

Figure Captions List

Figure 1. Sketch of mechanisms during foam infiltration into saturated sand.

Figure 2. Definition sketch of penetration zone and piezometric head during foam penetration (set-up described in Zheng et al., 2021).

Figure 3. Experimental results of the water discharge against square root of time (data from Zheng et al., 2021)

Figure 4. Grain / Bubble size distribution curves of the sands / foams (data from Zheng et al., 2021).

Figure 5. Principle of the bubble deformation during foam penetration of a pore throat.

Figure 6. Possible conditions when foam bubbles penetrate through pore throats.

Figure 7. Measured water retention curves with van Genuchten model fit (a) and the distribution curve of the throat diameter for each sand (b).

Figure 8. Calculated permeabilities and specific discharge as a function of infiltration depth (data from Zheng et al., 2021).

Figure 9. Penetration depth against time from experiments compared to model results.

Figure 10. Permeabilities used in model simulation.

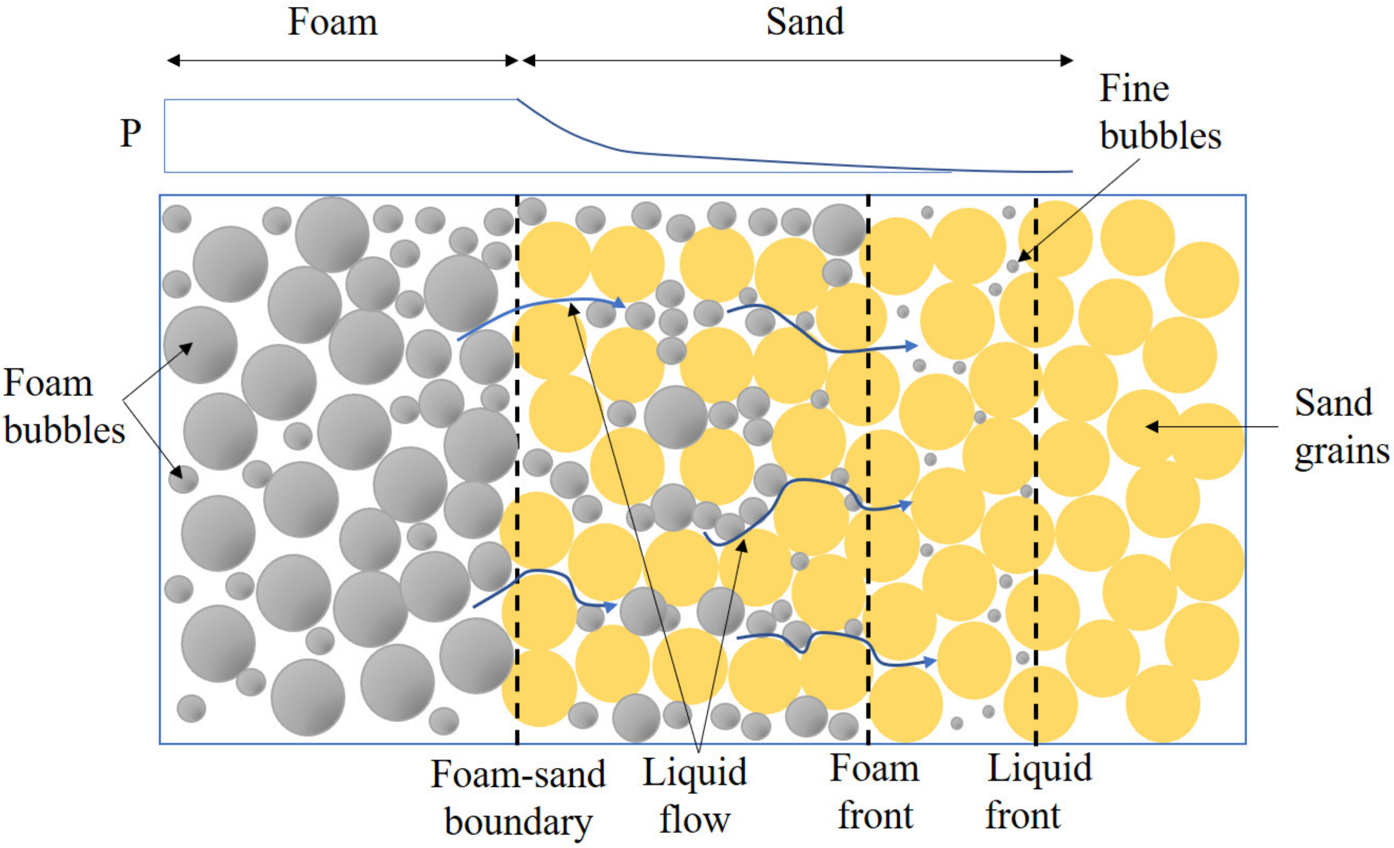
Foam
Sand
P
Fine bubbles
Foam bubbles
Sand grains
Foam-sand boundary
Liquid flow
Foam front
Liquid front

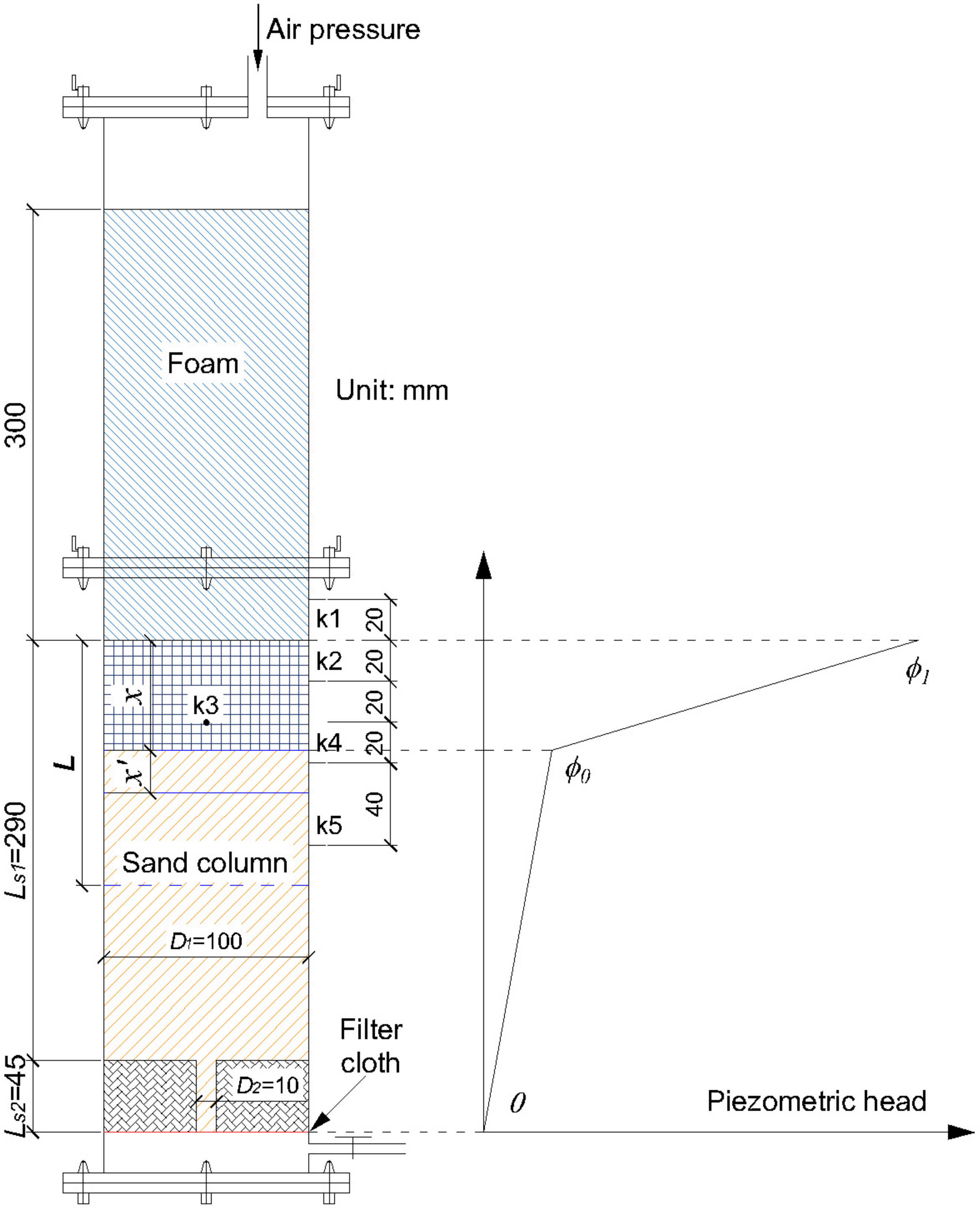
Air pressure
Foam
Unit: mm
300
k1
k2
k3
k4
k5
20
20
20
20
40
x
x'
L
L_{s1}=290
Sand column
D_1=100
L_{s2}=45
D_2=10
Filter cloth
ϕ_1
ϕ_0
0
Piezometric head

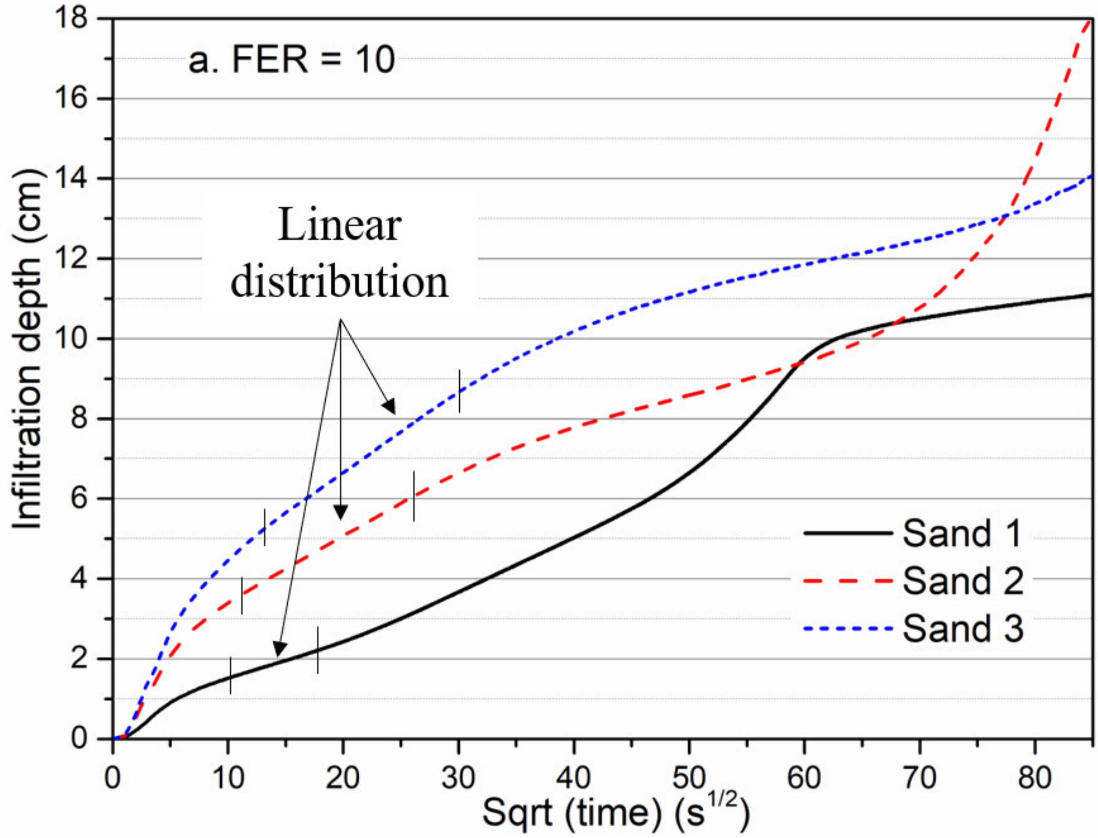
a. FER = 10
Linear distribution
Infiltration depth (cm)
Sqrt (time) ($s^{1/2}$)
0
2
4
6
8
10
12
14
16
18
0
10
20
30
40
50
60
70
80
Sand 1
Sand 2
Sand 3

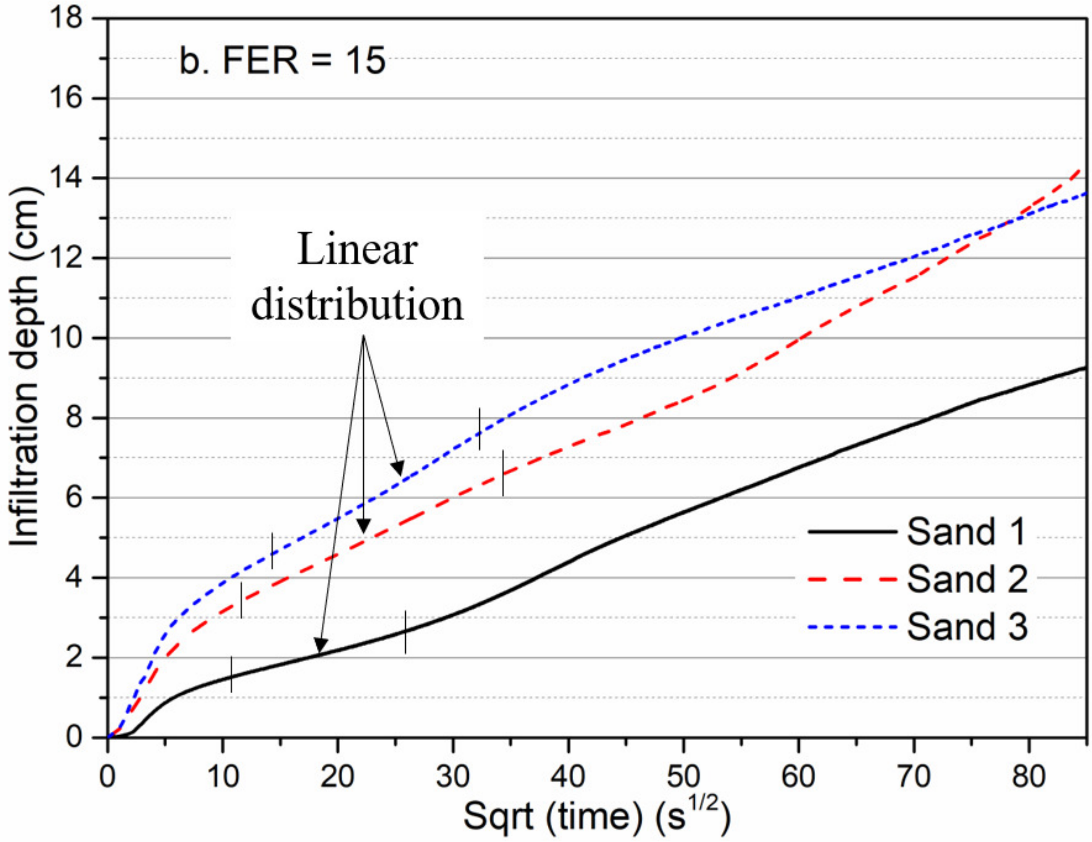

Figure 3b.tif Figure

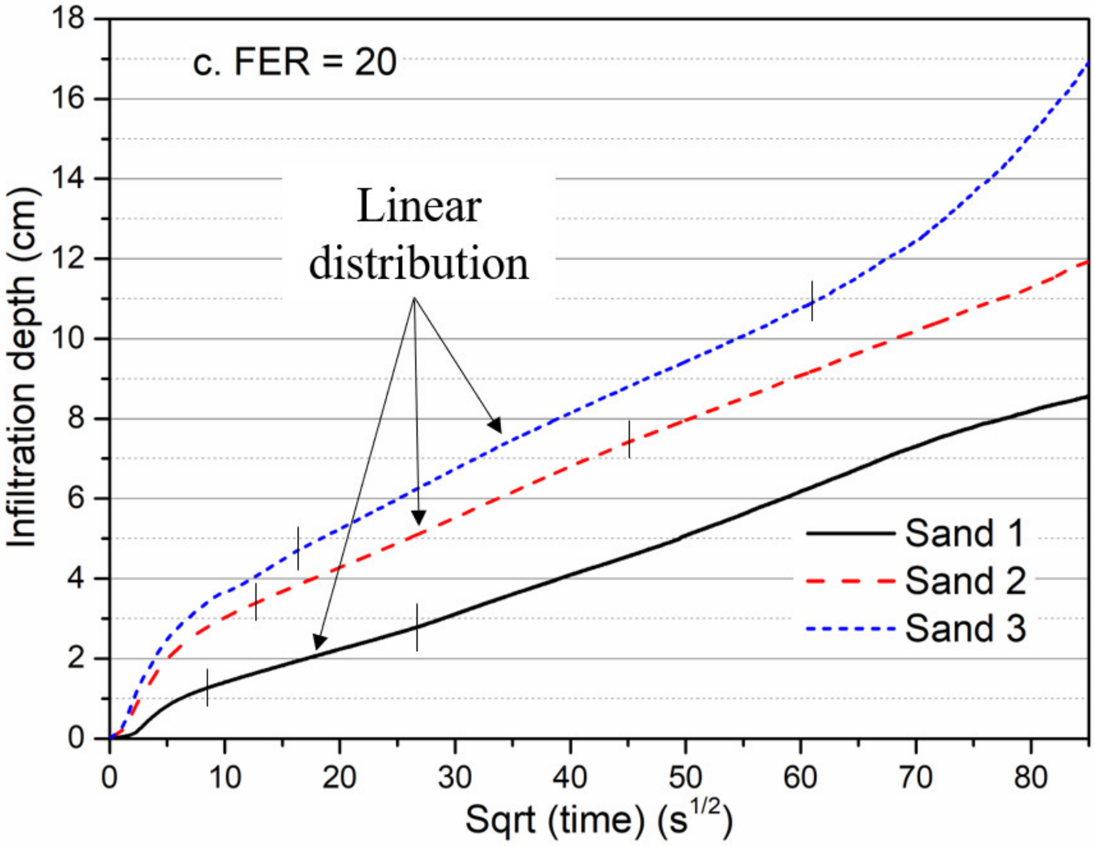
c. FER = 20
Linear distribution
Infiltration depth (cm)
Sqrt (time) ($s^{1/2}$)
Sand 1
Sand 2
Sand 3
0
2
4
6
8
10
12
14
16
18
0
10
20
30
40
50
60
70
80

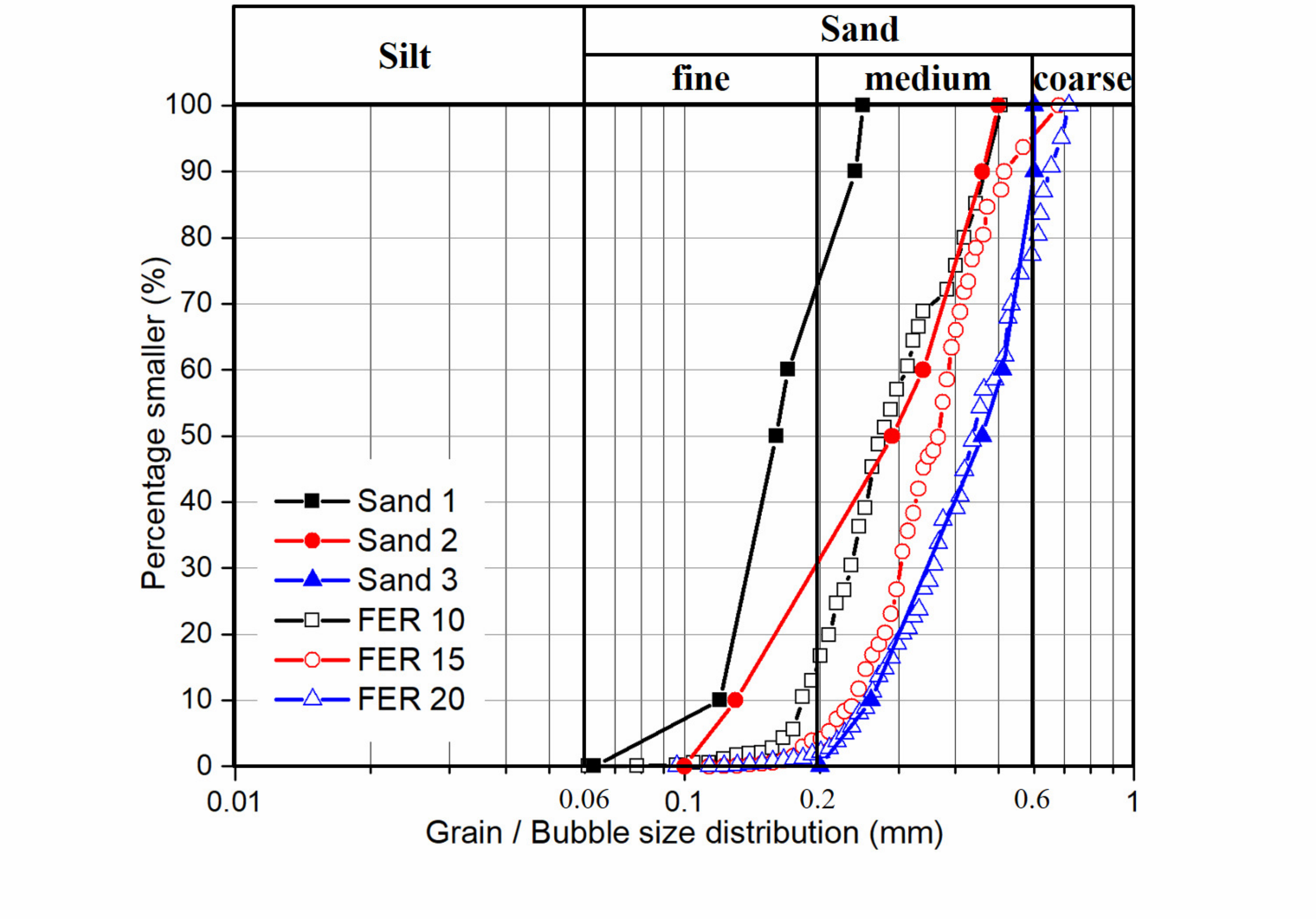
Silt
Sand
fine
medium
coarse
Percentage smaller (%)
0
10
20
30
40
50
60
70
80
90
100
0.01
0.06
0.1
0.2
0.6
1
Grain / Bubble size distribution (mm)
Sand 1
Sand 2
Sand 3
FER 10
FER 15
FER 20

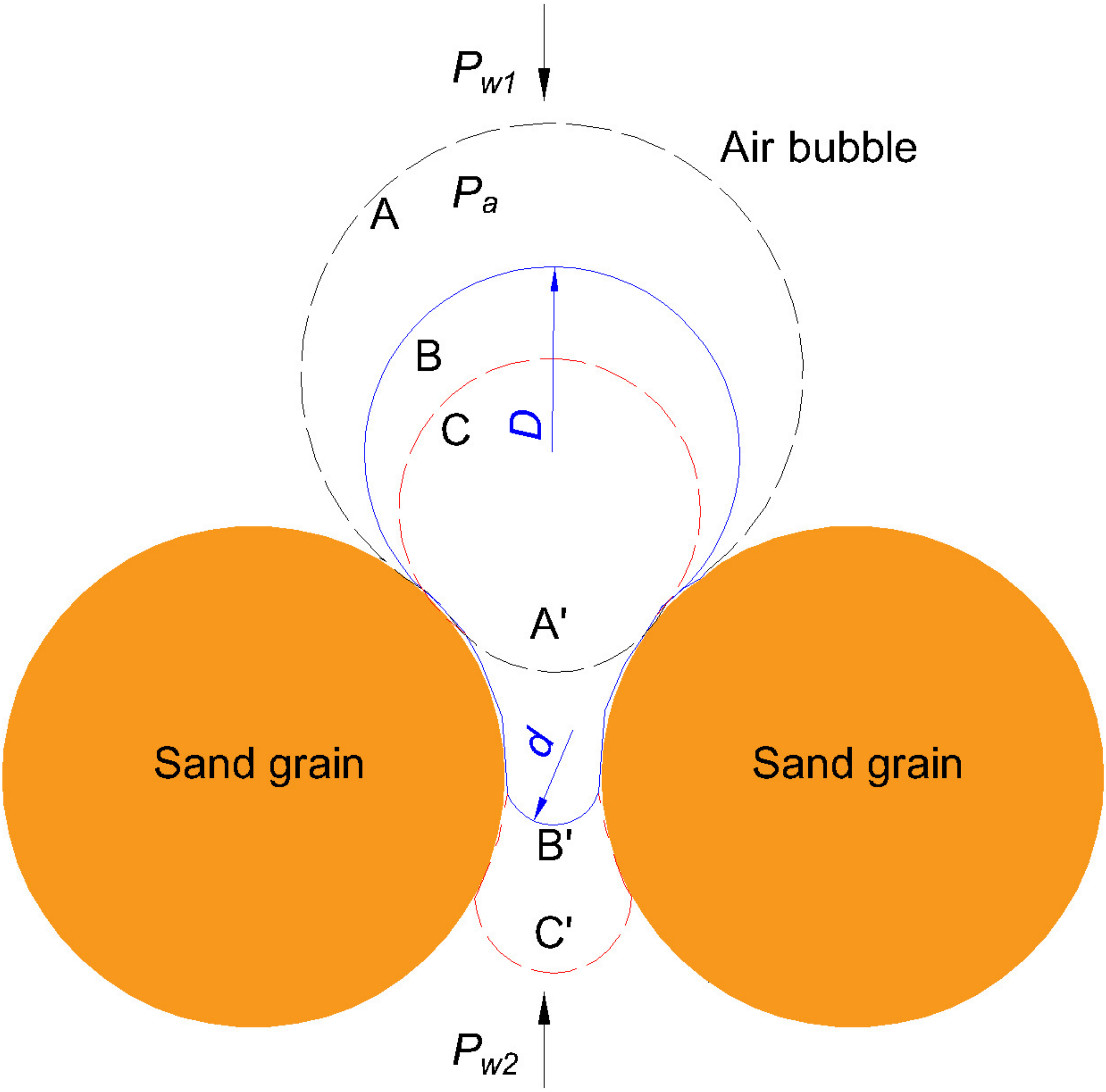

P_{w1}
Air bubble
A
P_a
B
C
D
A'
Sand grain
Sand grain
d
B'
C'
P_{w2}

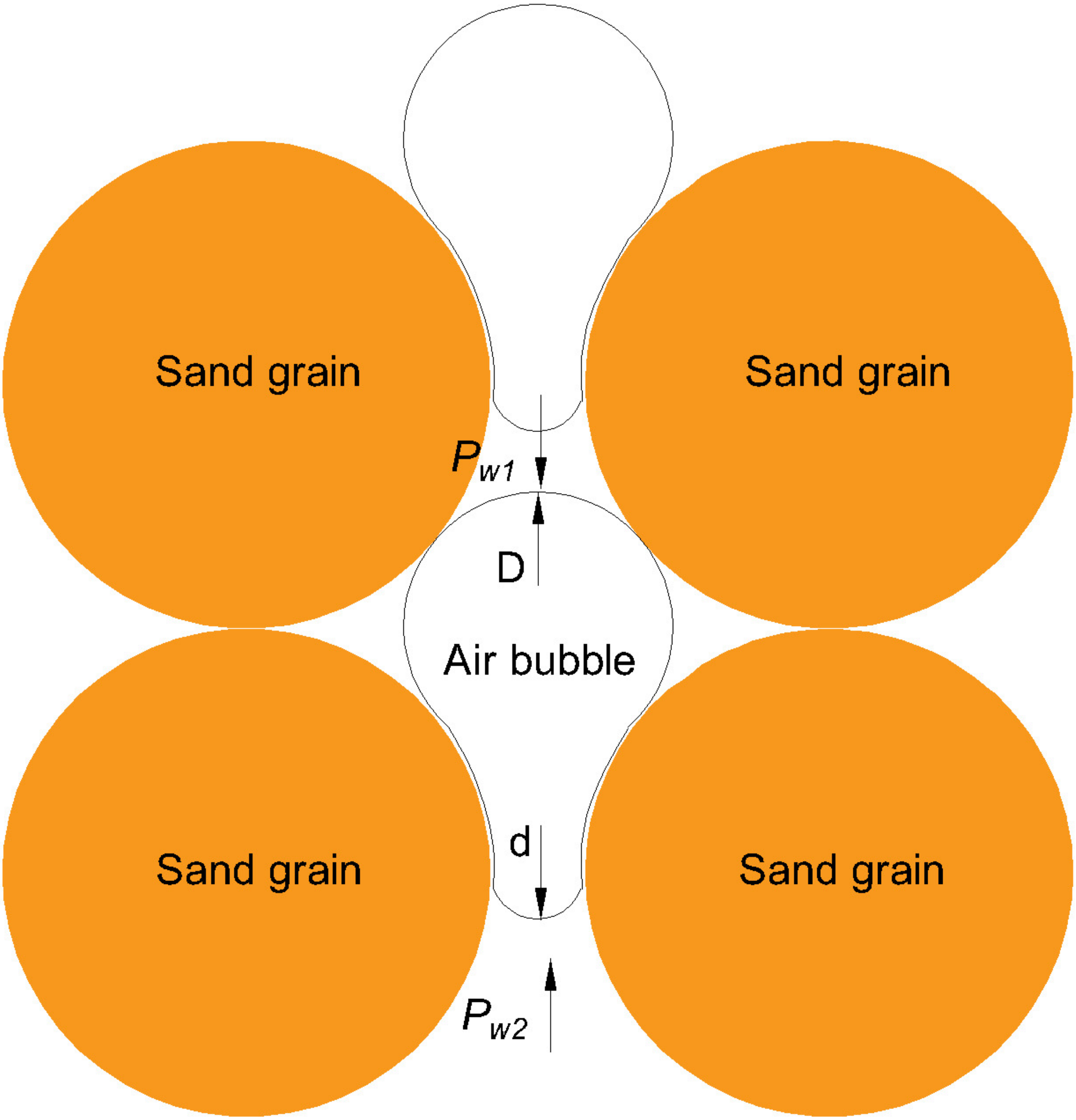
Sand grain
Sand grain
Pw1
D
Air bubble
d
Sand grain
Sand grain
Pw2

a

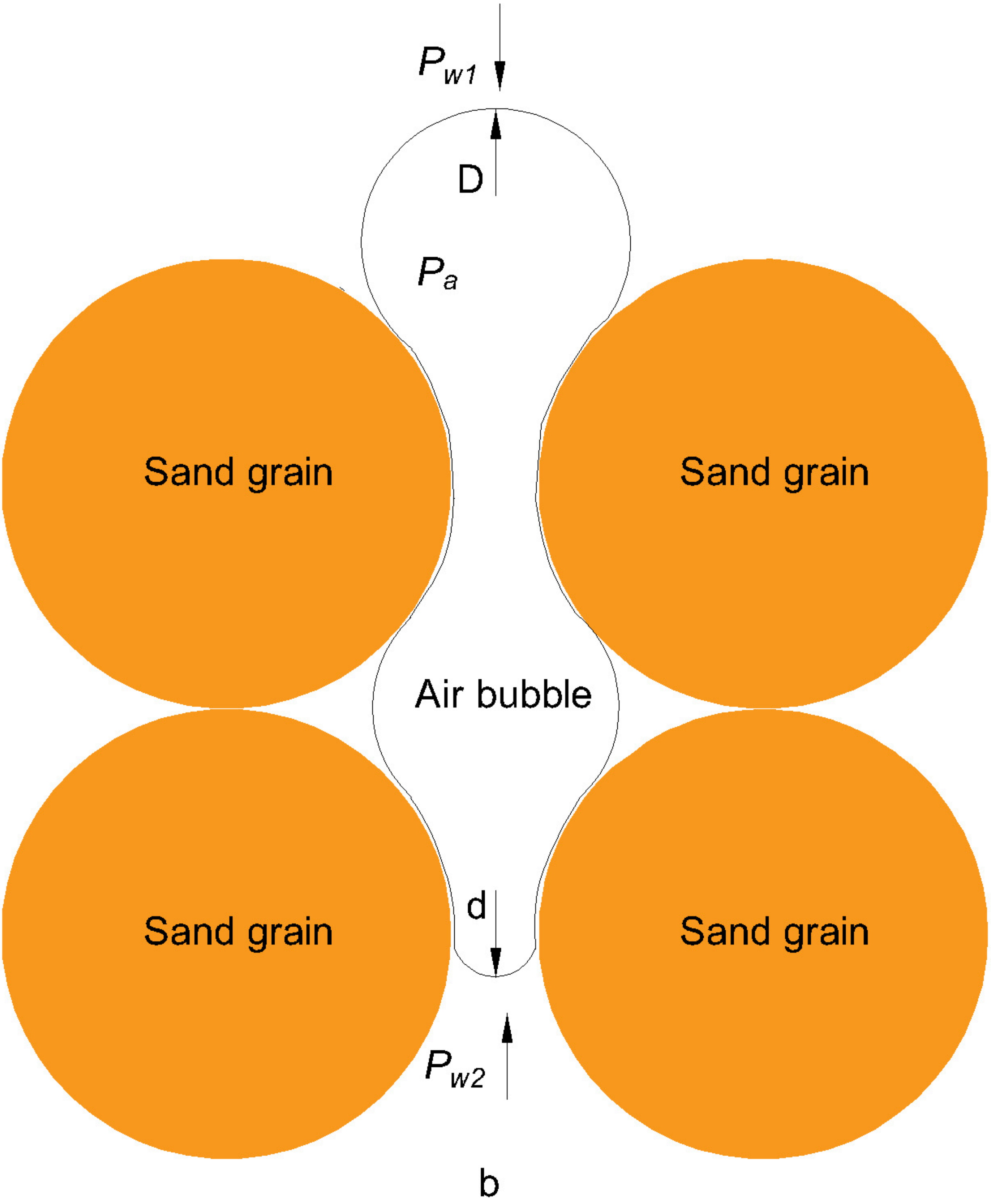

Figure 6b.tif *Figure*

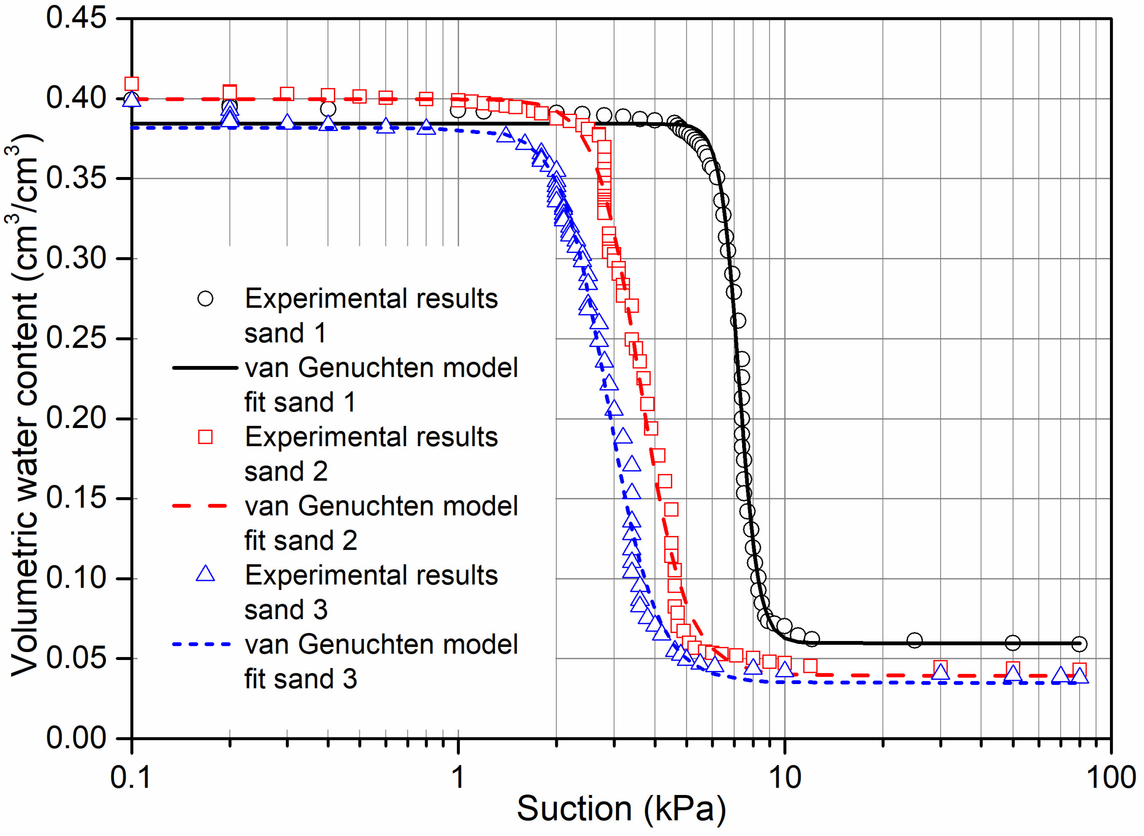
0.45
0.40
0.35
0.30
0.25
0.20
0.15
0.10
0.05
0.00
Volumetric water content (cm³/cm³)
0.1
1
10
100
Suction (kPa)
○ Experimental results sand 1
van Genuchten model fit sand 1
□ Experimental results sand 2
van Genuchten model fit sand 2
△ Experimental results sand 3
van Genuchten model fit sand 3

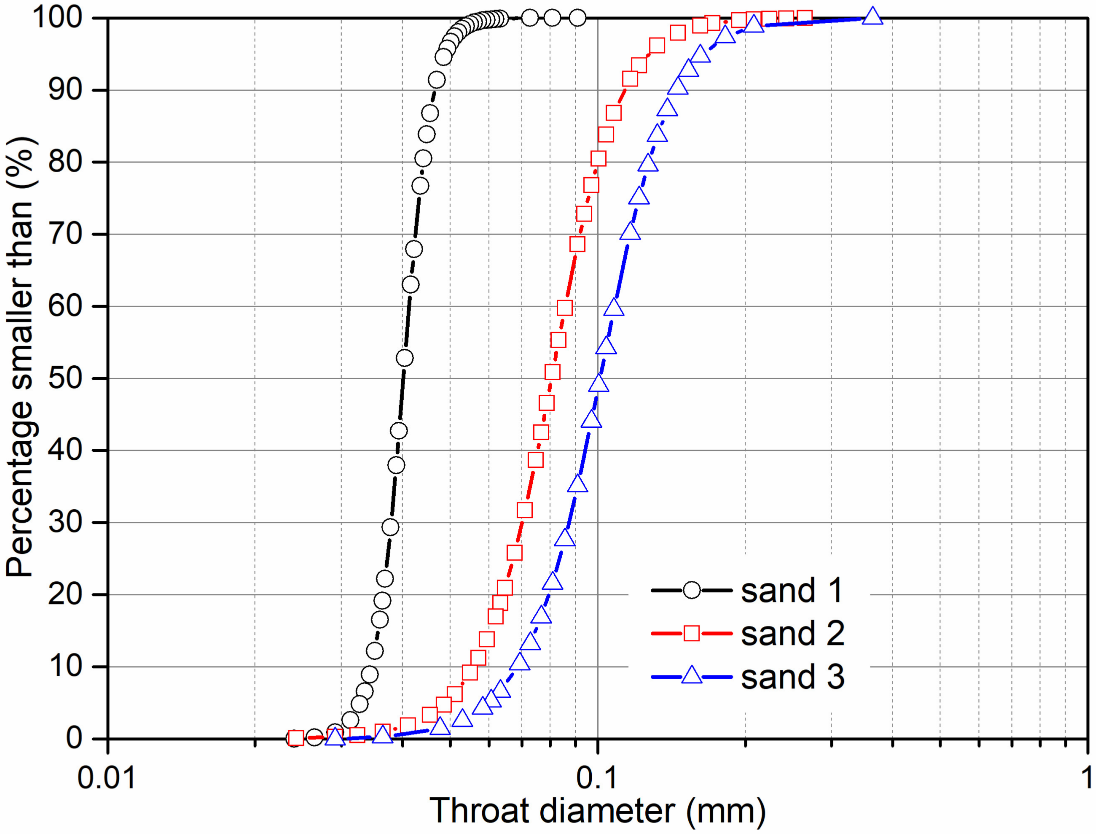
100
90
80
70
60
50
40
30
20
10
0
Percentage smaller than (%)
0.01
0.1
1
Throat diameter (mm)
sand 1
sand 2
sand 3

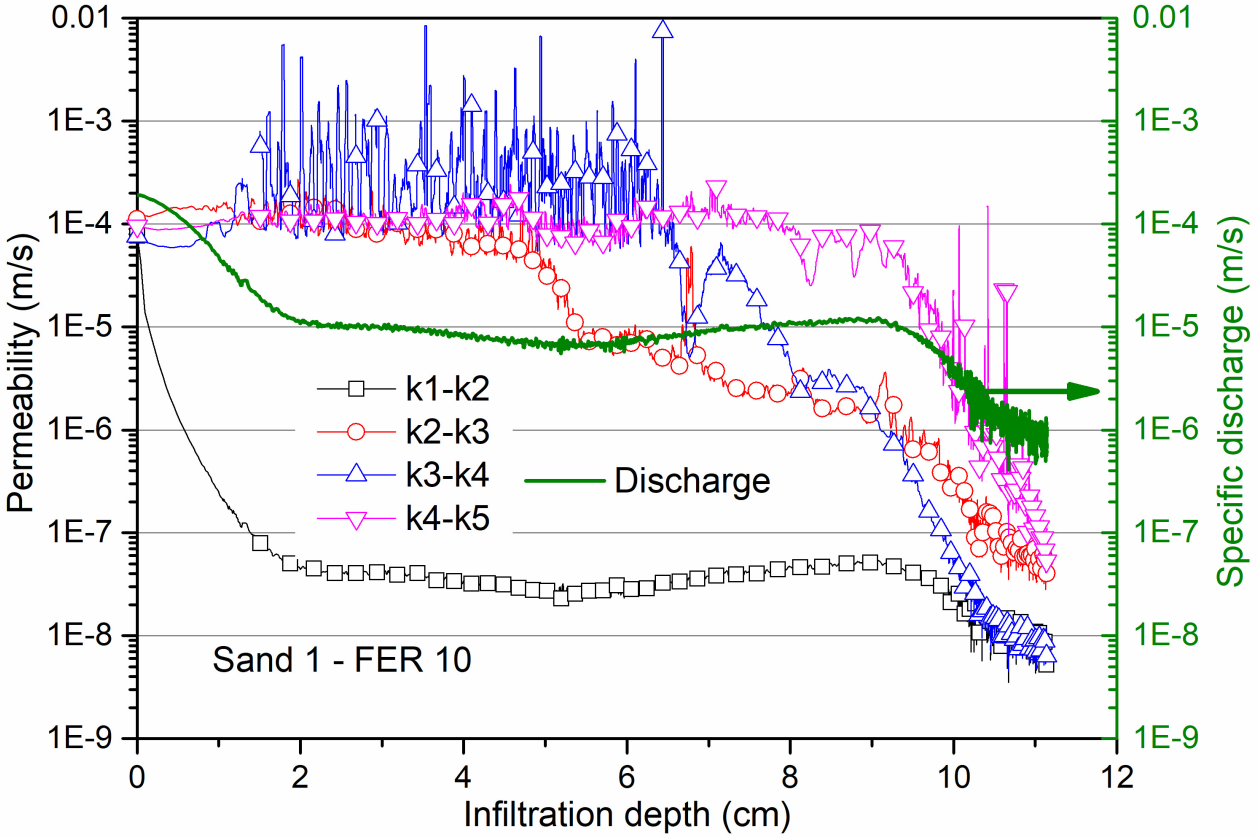
0.01
1E-3
1E-4
1E-5
1E-6
1E-7
1E-8
1E-9
Permeability (m/s)
0
2
4
6
8
10
12
Infiltration depth (cm)
Specific discharge (m/s)
k1-k2
k2-k3
k3-k4
k4-k5
Discharge
Sand 1 - FER 10

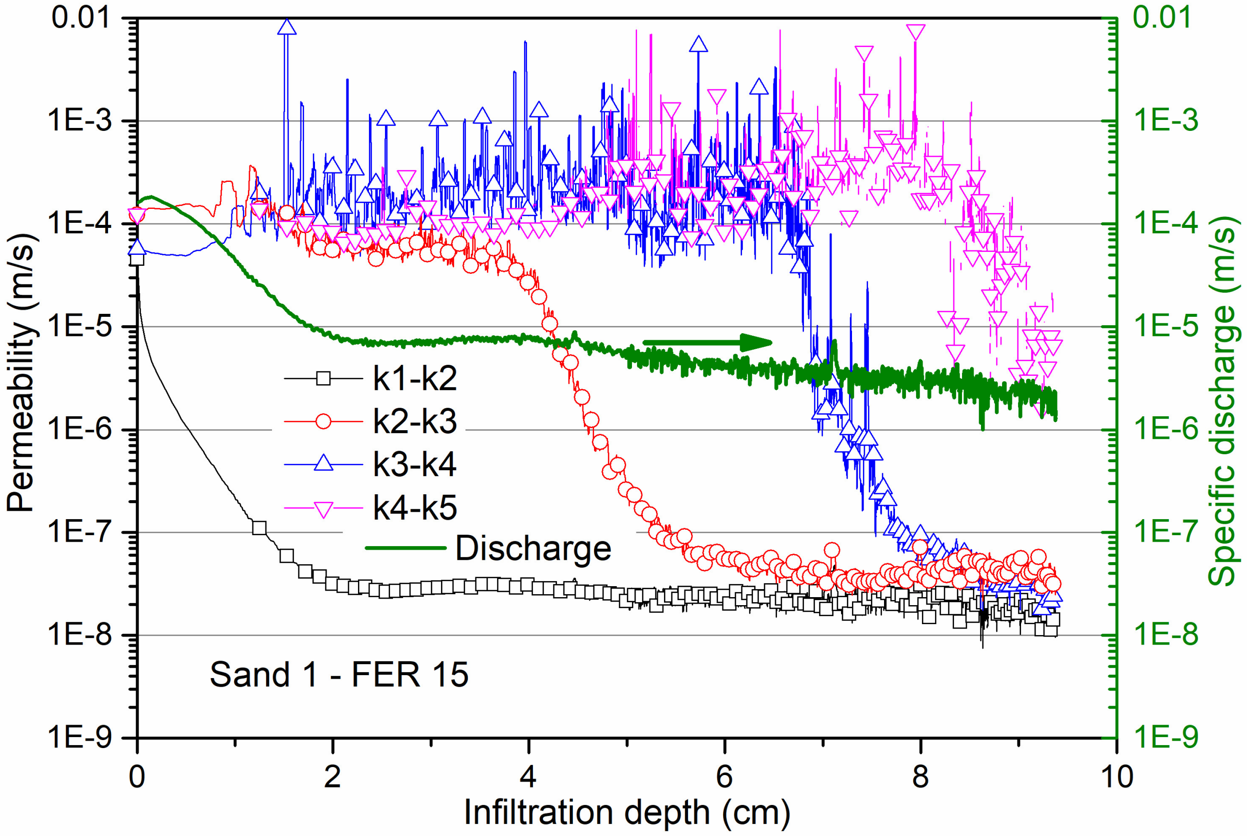
0.01
1E-3
1E-4
1E-5
1E-6
1E-7
1E-8
1E-9
Permeability (m/s)
Specific discharge (m/s)
0
2
4
6
8
10
Infiltration depth (cm)
k1-k2
k2-k3
k3-k4
k4-k5
Discharge
Sand 1 - FER 15

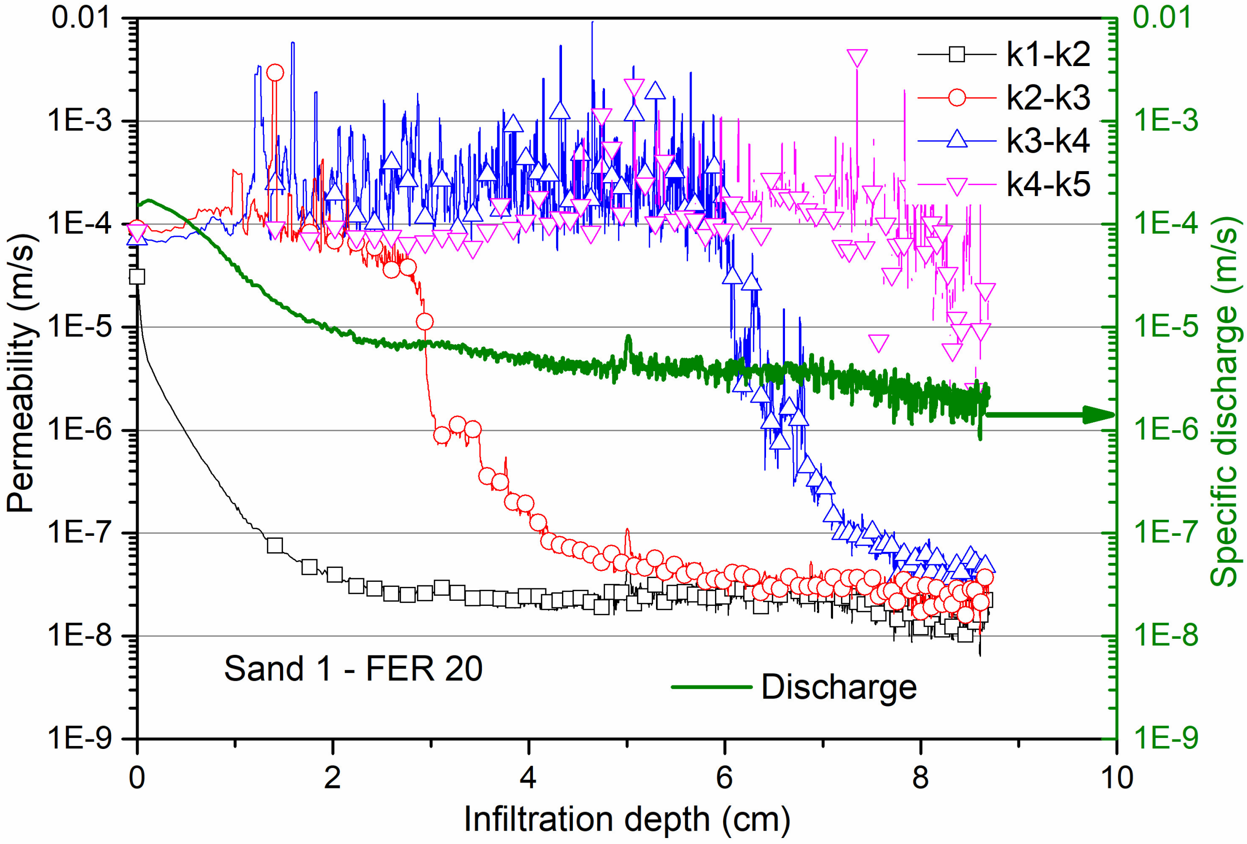
0.01
1E-3
1E-4
1E-5
1E-6
1E-7
1E-8
1E-9
Permeability (m/s)
Specific discharge (m/s)
0
2
4
6
8
10
Infiltration depth (cm)
k1-k2
k2-k3
k3-k4
k4-k5
Sand 1 - FER 20
Discharge

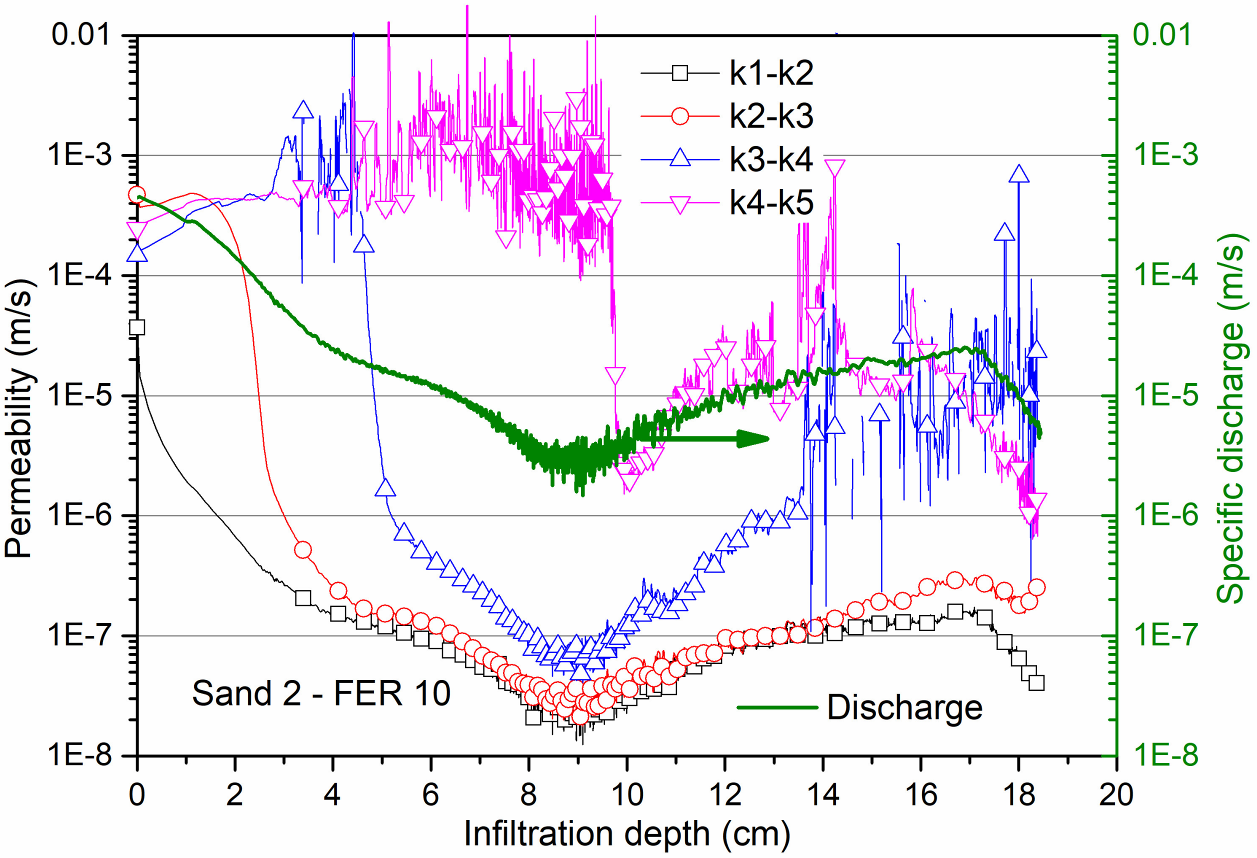
0.01
1E-3
1E-4
1E-5
1E-6
1E-7
1E-8
Permeability (m/s)
Specific discharge (m/s)
0
2
4
6
8
10
12
14
16
18
20
Infiltration depth (cm)
k1-k2
k2-k3
k3-k4
k4-k5
Sand 2 - FER 10
Discharge

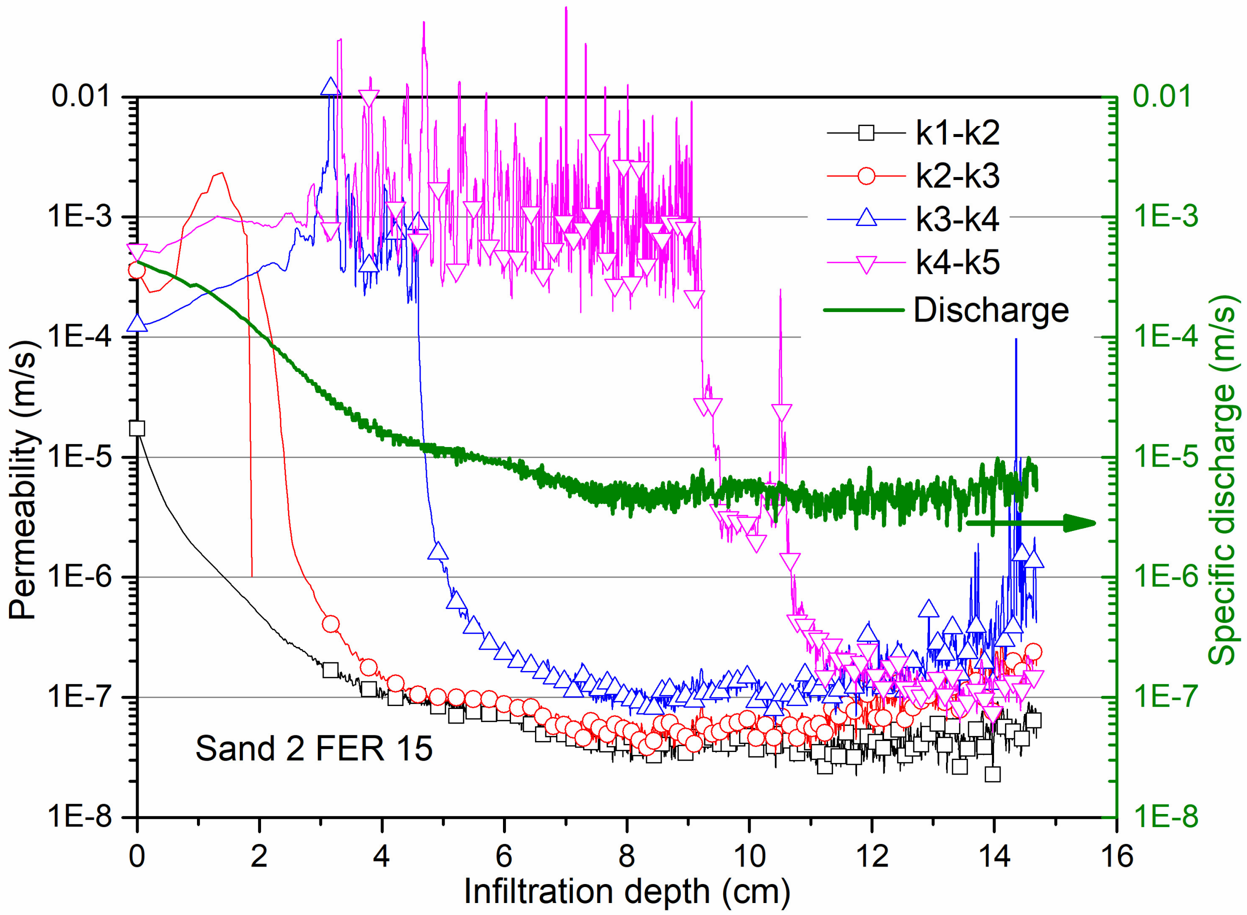
0.01
1E-3
1E-4
1E-5
1E-6
1E-7
1E-8
Permeability (m/s)
Specific discharge (m/s)
0
2
4
6
8
10
12
14
16
Infiltration depth (cm)
k1-k2
k2-k3
k3-k4
k4-k5
Discharge
Sand 2 FER 15

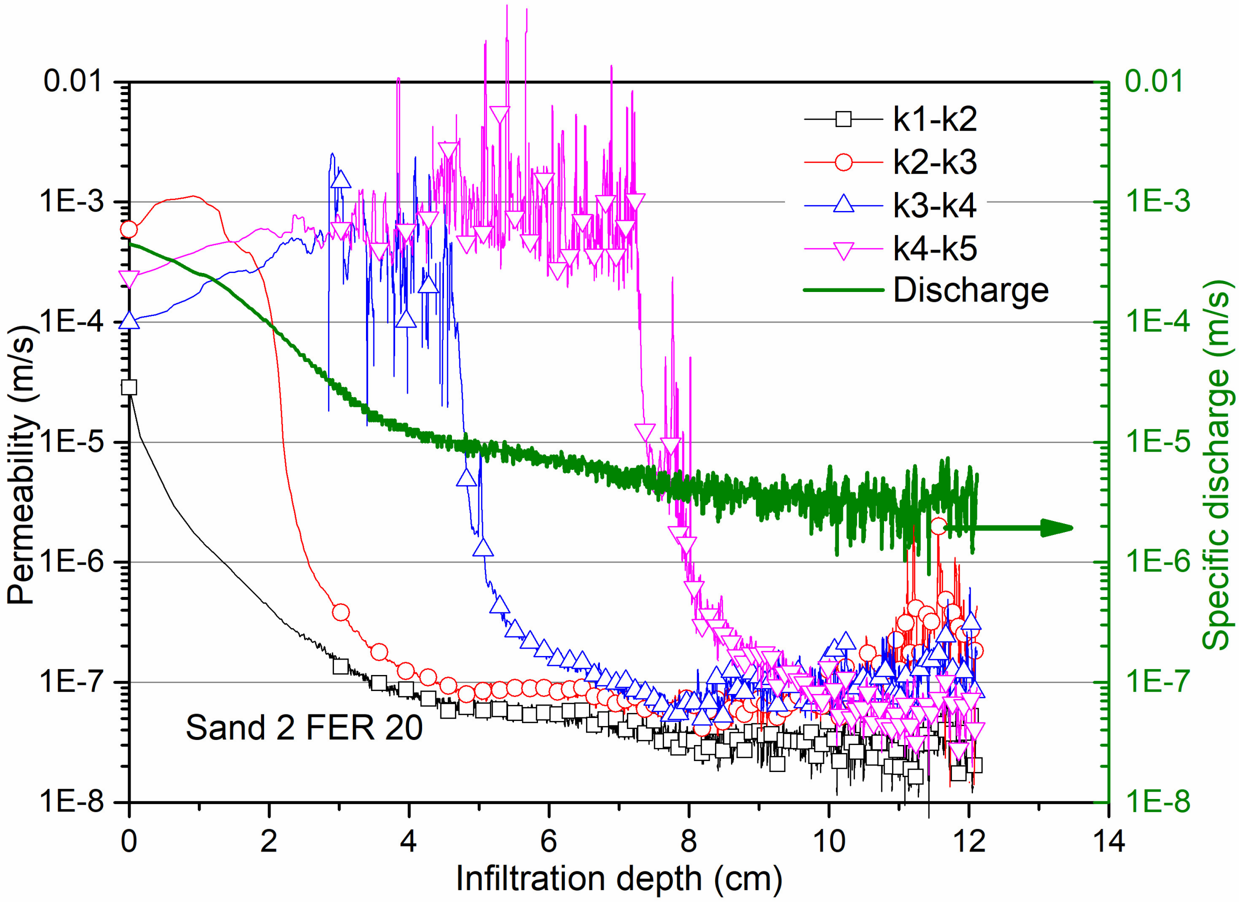
0.01
1E-3
1E-4
1E-5
1E-6
1E-7
1E-8
Permeability (m/s)
Specific discharge (m/s)
0
2
4
6
8
10
12
14
Infiltration depth (cm)
k1-k2
k2-k3
k3-k4
k4-k5
Discharge
Sand 2 FER 20

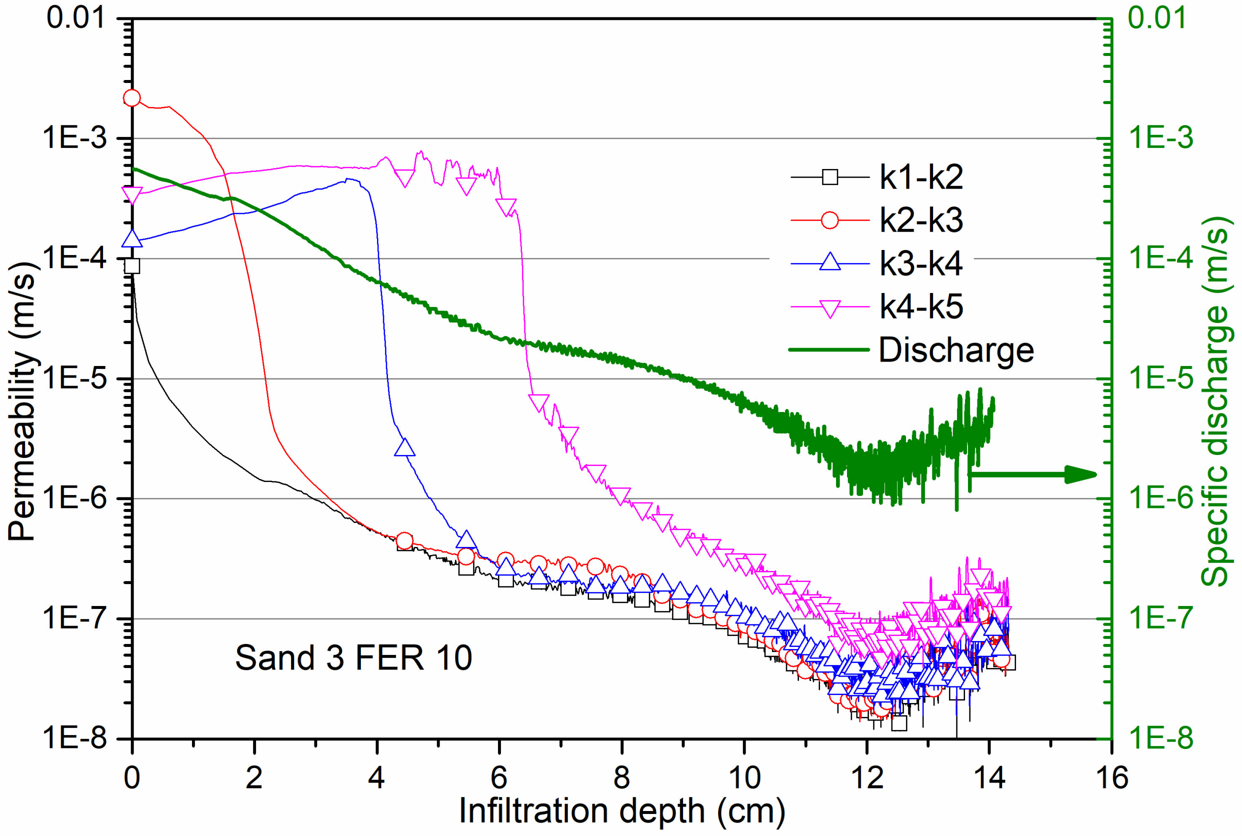
0.01
1E-3
1E-4
1E-5
1E-6
1E-7
1E-8
Permeability (m/s)
0
2
4
6
8
10
12
14
16
Infiltration depth (cm)
Specific discharge (m/s)
k1-k2
k2-k3
k3-k4
k4-k5
Discharge
Sand 3 FER 10

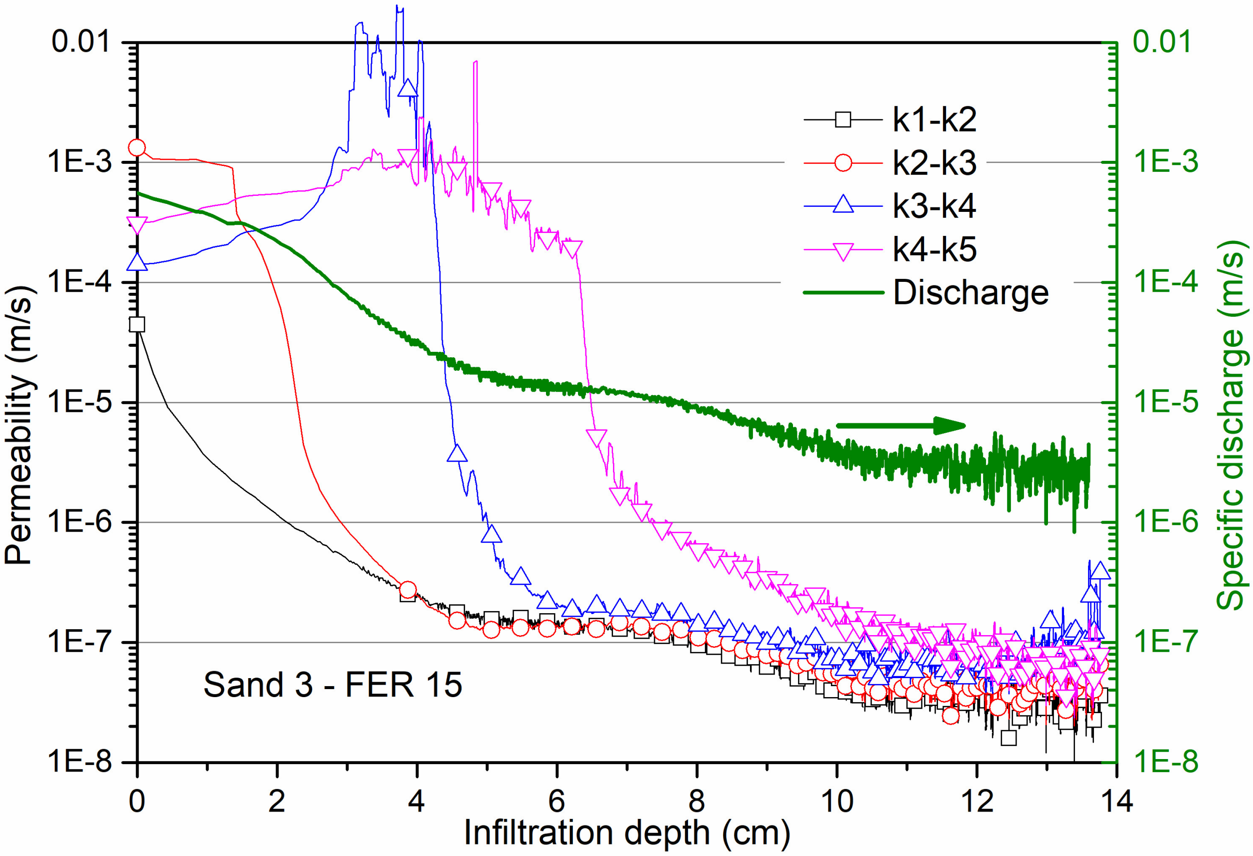
0.01
1E-3
1E-4
1E-5
1E-6
1E-7
1E-8
Permeability (m/s)
0
2
4
6
8
10
12
14
Infiltration depth (cm)
Specific discharge (m/s)
k1-k2
k2-k3
k3-k4
k4-k5
Discharge
Sand 3 - FER 15

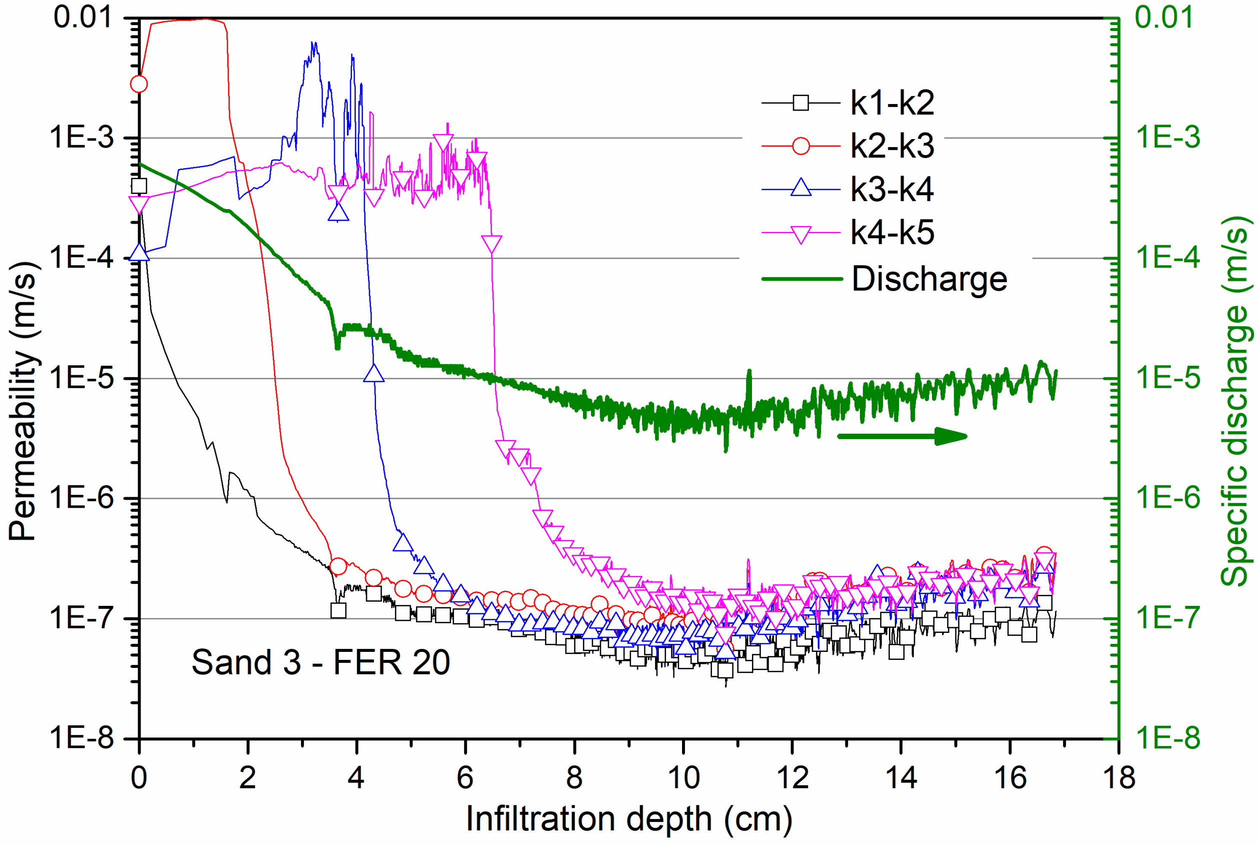
0.01
1E-3
1E-4
1E-5
1E-6
1E-7
1E-8
Permeability (m/s)
Specific discharge (m/s)
0
2
4
6
8
10
12
14
16
18
Infiltration depth (cm)
k1-k2
k2-k3
k3-k4
k4-k5
Discharge
Sand 3 - FER 20

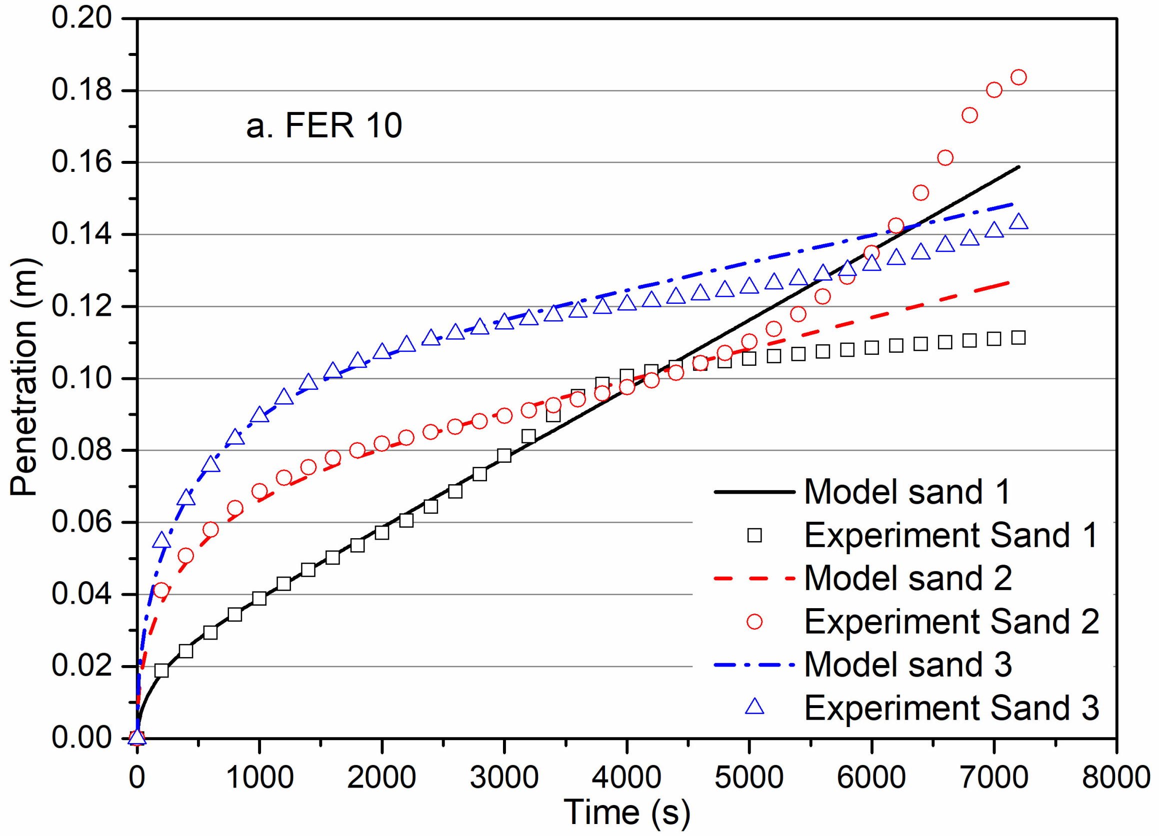
a. FER 10
Penetration (m)
0.00
0.02
0.04
0.06
0.08
0.10
0.12
0.14
0.16
0.18
0.20
Time (s)
0
1000
2000
3000
4000
5000
6000
7000
8000
Model sand 1
Experiment Sand 1
Model sand 2
Experiment Sand 2
Model sand 3
Experiment Sand 3

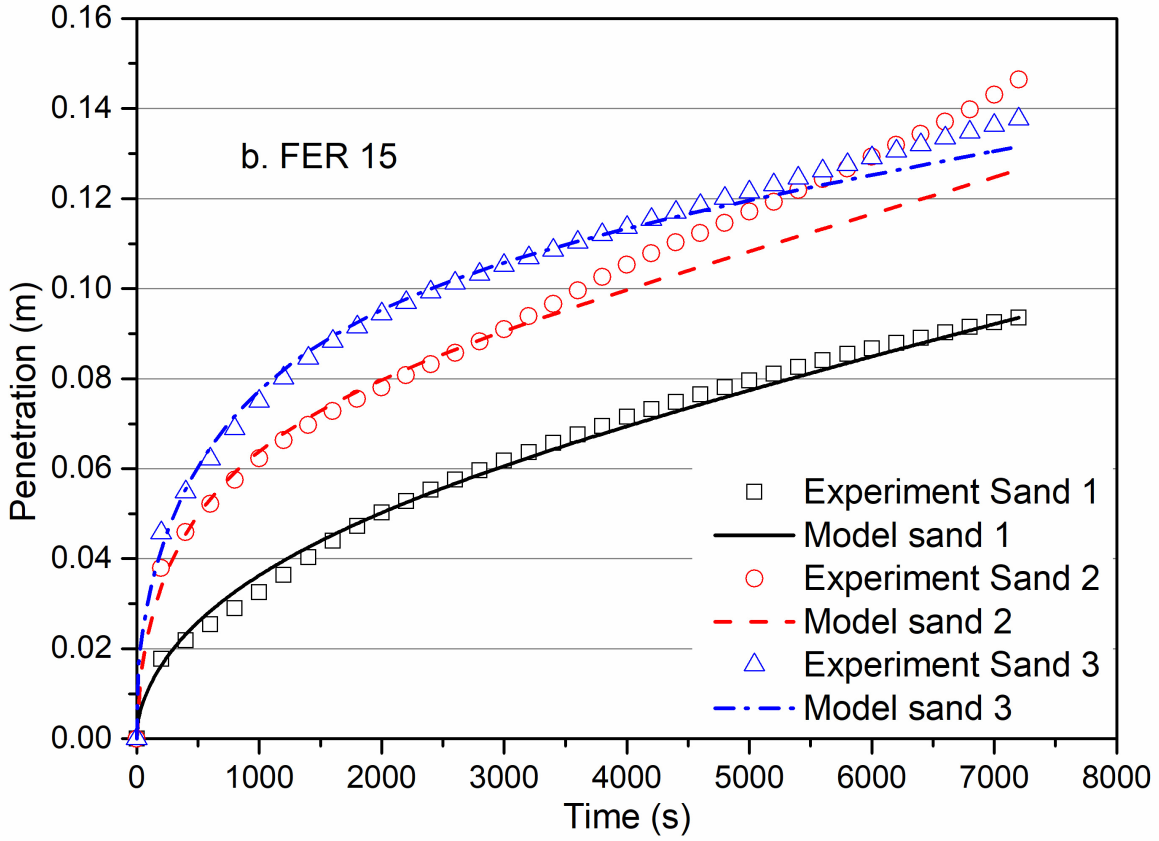
b. FER 15
Penetration (m)
0.00
0.02
0.04
0.06
0.08
0.10
0.12
0.14
0.16
Time (s)
0
1000
2000
3000
4000
5000
6000
7000
8000
□ Experiment Sand 1
Model sand 1
○ Experiment Sand 2
Model sand 2
△ Experiment Sand 3
Model sand 3

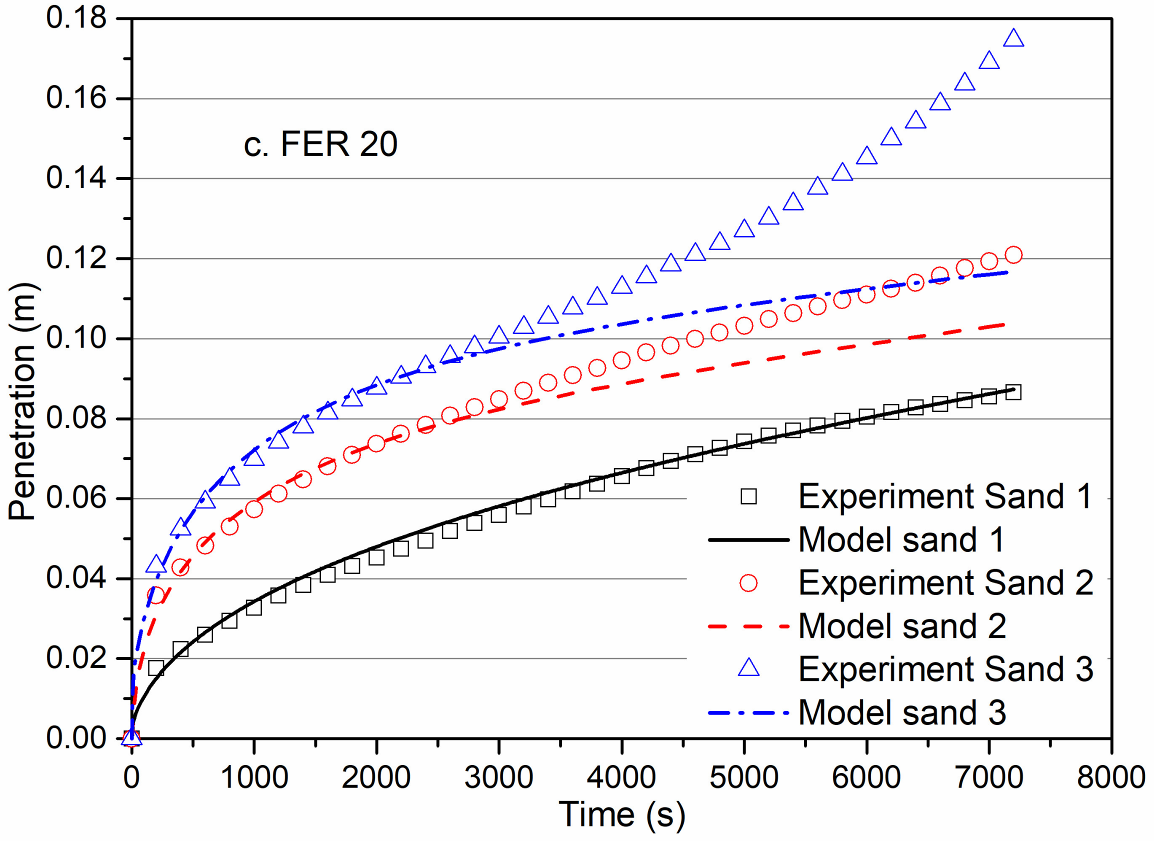
c. FER 20
Penetration (m)
0.00
0.02
0.04
0.06
0.08
0.10
0.12
0.14
0.16
0.18
Time (s)
0
1000
2000
3000
4000
5000
6000
7000
8000
Experiment Sand 1
Model sand 1
Experiment Sand 2
Model sand 2
Experiment Sand 3
Model sand 3

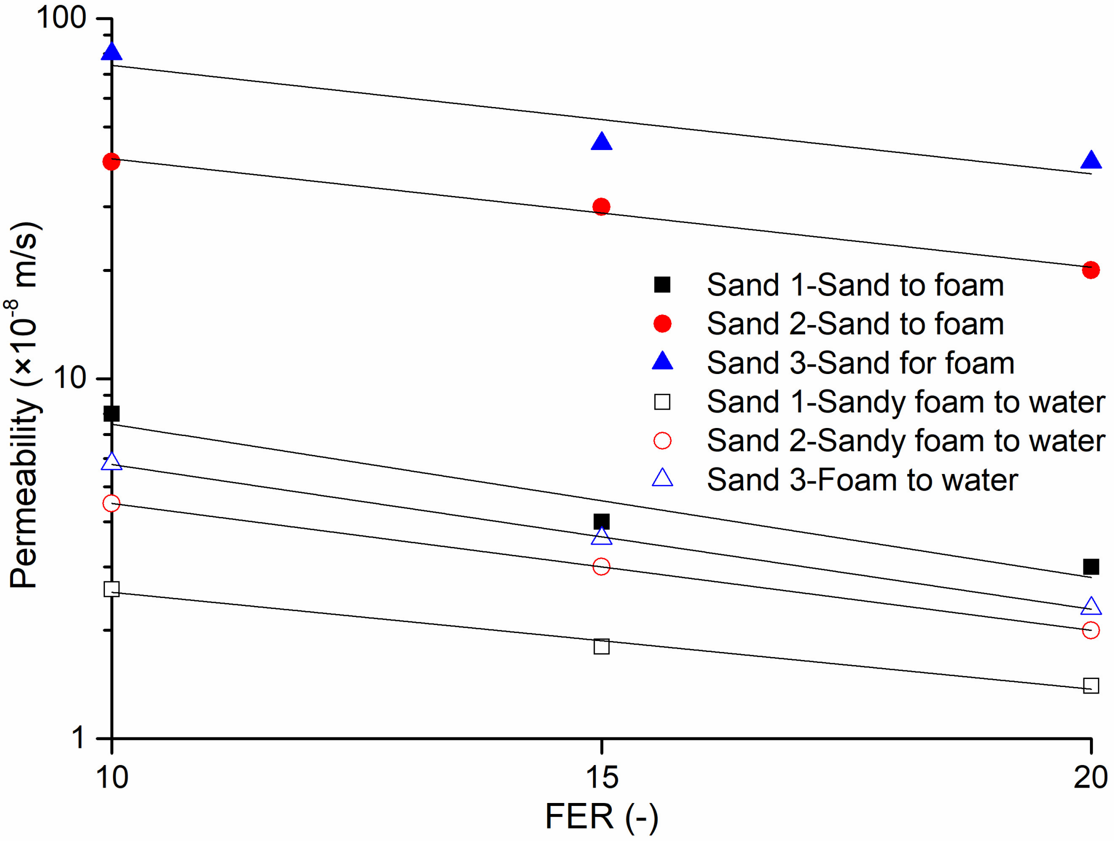

Figure 10.tif Figure